PHOTOMETRIC CALIBRATION OF THE FAINT OBJECT SPECTROGRAPH

J. D. Neill, R. C. Bohlin, and G. Hartig
Space Telescope Science Instititute

FOS Instrument Science Report CAL/FOS-077
April 1992

Abstract

The absolute photometric calibration of the Faint Object Spectrograph (FOS) is derived from observations of three spectrophotometric standard stars (BD+28D4211, BD+75D325, and HZ-44) in the large 4.3″ entrance aperture for 14 detector-disperser combinations (six for the blue digicon, eight for the red). Observations of the three stars are used from five epochs between 1991.4 and 1992.0 for each of the blue and red digicons. Absolute calibrations for the four smaller single entrance apertures are computed from a set of transmission measurements relative to the 4.3″ aperture at one epoch for each side. Observations that span the time interval from 1991.0 to 1992.2 show a decrease in the sensitivity for the blue digicon of about 10% per year at all wavelengths, while the red digicon has a sensitivity that is constant to 5%, except in the wavelength range of 1800-2100Å where the decrease in sensitivity is also roughly 10% per year.

I. Introduction

Each spectrophotographic mode has an absolute calibration or inverse sensitivity (S^{-1}) that can be used to derive the flux of a point source by $F = S^{-1} * C$, where F is the flux of the source and C is the observed counts per second. The S^{-1} curve can be calculated from the count rates of stars with known fluxes.

The original S^{-1} curves were derived from labratory sources while the FOS was on the ground. During the early phase of HST orbital science verification, spanning the time from 1990.9 to 1991.0, observations of standard stars generated the first set of S^{-1} curves from flight data. Since mid-1991, the focus of the observatory has stablized and, the geomagnetic image motion (GIM) problem has been addressed (Hartig *et al* 1992). The current set of S^{-1} curves presented here is derived from observations of three standard stars between 1991.4 and 1992.0. This 1991.4 - 1992.0 calibration differs from the 1990.9 - 1991.0 set by a maximum of 20% and will be used for the complete reprocessing of the archive that is scheduled to begin soon. Table 1 lists the observations used for the derivation of the on-orbit calibrations; Table 2 contains the detector-disperser combinations used to obtain these observations; and Table 3 lists the apertures through which these observations were made (see below).

II. Standard Star Selection and Observation

Five standard stars are selected from the IUE standards of Bohlin *et al* (1990). The three stars BD+75D325, BD+33D2642, and BD+28D411 have been used to monitor the changes in IUE sensitivity and have the best measured UV flux distributions. The star G191B2B (WD0501+527) is selected because of its well determined flux and a featureless continuum that is used to determine the FOS flat field correction (Keyes, 1992). The star HZ-44 is selected to extend the magnitude range to 9.5 - 11.8 in the V band. The fluxes of these stars at visual wavelengths were measured by Oke (1990).

The currently available set of 210 observations is presented in Table 1. Column one is the rootname of the Generic Edited Information Set (GEIS) for the observation. Column two gives the proposal identification number. Columns three through five contain the configuration of the FOS used for the observation. Column six is the target star name. Column seven is the date of the observation in fractional years. The table is also subdivided into seven groups. The first group consists of the 61 observations that were used in producing the S^{-1} curves that were delivered to the Calibration Data Base (CDBS) on the 30th of March, 1992. The remaining groups are of insufficient quality or were obtained too recently to be included for this delivery. The second group of observations could not be used due to a target acquisition failure. The third group consists of good quality observations of the standard star BD+33D2642 that are rejected, because the published flux for this object produces S^{-1} curves that systematically disagree with those generated from the remaining standard stars (see section IV). The fourth group was taken early in the HST mission when the focus of the HST was changed several times during experiments to determine the optimum focus. The fifth group was received after the 1992 Mar 30 delivery to CDBS. The sixth group consists of observations of BD+75D325 through the single apertures and is used to calculate the throughput ratios with respect to the 4.3″ aperture. The 4.3″ aperture observations from this set are included in group 1 and are not repeated in group 6. The seventh and final group consists of observations of BD+28D4211 with the paired apertures for use in calculating throughput ratios for these apertures as part of our ongoing FOS calibration effort.

A single measurement of the FOS sensitivity is calculated from an observation of one of the program stars using a unique combination of digicon, disperser, and the 4.3″ aperture. Each observation has an overscan value of 5 and an nxstep value of 4. The nxstep value of 4 defines the pixel subsampling with respect to the diode resolution elements at four pixels per diode, i.e. 12.5 micron substeps and 50 micron wide diodes. To avoid loss of light due to the GIM offset in the y direction (Hartig *et al* 1992), three ysteps are centered on the nominal ybase with a spacing of 10.67 ybase units (8.33 microns). Observations in Table 1 before 1992.0 are accompanied by observations of a wavelength calibration lamp and are used to accurately determine the wavelength scale. Hereafter, these observations will be refered to as wavecals.

Each observation is converted from raw counts to counts per second, de-GIMed, corrected for detector non-linearity (Lindler and Bohlin, 1988), and flat fielded (Anderson, 1992) to yield the observed count rate. The standard data quality array is used in later steps to avoid bad data points. A scattered light component is subtracted before the flat field division for observations with the blue digicon using the G130H, or G160L dispersers and observations with the red digicon using the G190H, G780H, G160L, G650L, or PRISM dispersers. These configurations have regions where the response to dispersed light is zero and where the residual background and scattered light can be measured. For other configurations, the scattered light can not be measured, because the response is always greater than zero but adds a sytematic error of less than 1% to the S^{-1} curves for these configurations. To remove the small-scale effects of the pixel-to-pixel response which varies over time in the wavelength region of 1800-2100Å on the red side, the flat field corrections (Keyes, 1992) for the G190H, G270H, and G160L dispersers is linearly interpolated in time between bracketing flat field observations. With the exception of the scattered light subtraction and the flat field interpolation, these steps are performed using standard CALFOS routines, which duplicate the routine post observation data processing system (PODPS) reductions.

The wavecals are reduced identically to the object observations and are used to shift the object count rate arrays to a template wavelength scale by cross- correlating the appropriate wavecal with a template wavecal. The shifts derived from this cross-correlation fall between ± 1 diode. These shifts are applied as an integer number of pixels to both the object countrate array and the data quality array. The mean shift for all the observations with wavecals is $+0.05$ diodes (0.2 px) with a standard deviation of ± 0.3 diodes (1.2 px). This small wavelength adjustment is most important for dispersers with steep wavelength cutoffs and for the PRISM whose dispersion is non-linear. Our investigations demonstrate that wavecals are not crucial to the absolute calibration program, and wavecals do not accompany absolute calibration observations after 1992.0.

III. Inverse Sensitivity Curves

a. Derivation

The S^{-1} curves are calculated from the 61 high quality observations in Table 1, group 1, for the 14 most useful detector-disperser combinations of the FOS (see Table 2) using the 4.3″ aperture. S^{-1} curves for the other single apertures (see Table 3) are calculated from these curves and the throughput ratios measured by the observations listed in Table 1, group 6. The paired aperture throughput ratios have not yet been calculated (see Table 1, group 7 and Table 3).

A single measurement of the S^{-1} for a given configuration is derived from the ratio of the known flux spectrum of the source in ergs s^{-1} cm^{-2} A^{-1} to the observed count rate spectrum. The observed count rate array is read and the three ysteps are examined. The ystep with the highest count rate is used for the calculation; and the other two ysteps are included if their countrate is within 0.5% of the highest ystep. For all dispersers except

the PRISM, the observed count rate distribution is resampled to match the published flux distribution using a trapezoidal integration with limits defined as the midpoints between the wavelengths of the standard star spectrum. The non-linear dispersion of the PRISM requires that the published flux distribution be resampled to match the count rate distribution wavelengths using the same technique. A bi-cubic spline is fit to the ratio points and the resulting spline coefficients are used to generate the S^{-1} curve over the required wavelength range. Node positions for the splines depend only on the disperser with the exception of G160L, which has different node positions for the blue and red digicon. In most cases, the nodes are placed at specific wavelengths to follow features in the sensitivity for the disperser but are sometimes evenly spaced across the wavelength range.

For dispersers that include wavelengths near 3200Å, a mask is employed to avoid the range 3100-3350Å, the region where the IUE measurements are joined to the ground based observations. The match is not always smooth in this region due to the low sensitivity of the IUE and the difficulty in obtaining ground based absolute fluxes.

Table 2 lists the detector-disperser combinations that are used in this program. Column one lists the dispersers used with the blue digicon and column two lists those used with the red digicon. The name in parentheses in these two columns is the alias for the disperser that appears in the headers of the observations and also in the figures for this paper. Column three lists the number of nodes used in fitting the S^{-1} curve for each disperser; and the number in parentheses is the number of nodes on the red side if not the same as on the blue side. An asterisk indicates that the nodes are specifically placed, otherwise the nodes are evenly placed in wavelength.

Table 3 lists the apertures used for this program. The first column is the designation that appears in the headers of the observations and also in the figures for this paper. The second column is the size of the aperture in arcsec. The third column is the shape of the aperture. The fourth column is either SINGLE or PAIRED.

To reduce systematic errors, multiple observations with the 4.3″ aperture are made of different program stars. Some configurations are better observed than others as shown in Table 1. Multiple S^{-1} curves for a given configuration are combined by averaging the S^{-1} curves generated from all the observations for that configuration. The data quality array is used to eliminate bad points from the average. Bad points are common on the ends of the S^{-1} curves because of the shifting due to the GIM and the wavecal cross-correlation. In these cases, neighboring good values are used to extrapolate a value for the end points. If points are missing elsewhere in the array, a value is interpolated from neighboring good values. Figure 1 shows the final averaged S^{-1} curves for each configuration in Table 2 using the 4.3″ aperture.

The set of S^{-1} curves for the smaller single apertures is generated by applying the throughput ratio for the given aperture with respect to the 4.3″ aperture. These ratios are calculated from the observations in Table 1, group 6. The ratios are fit with a polynomial

of order 1 as a function of wavelength, except the red side G190H configuration which is fit with a polynomial of order 2 due to stronger curvature in the aperture ratio function. The wavelength regions less than 1650Å on the red side G160L and less than 3800Å on the red side G650L are masked before fitting to avoid noise caused by slight mismatches near the sensitivity cutoffs. The fits are then applied to the 4.3″ S^{-1} curves as a function of wavelength to generate the four S^{-1} curves for the smaller single apertures for each configuration.

Table 4 is the average of the fits to the ratio points for each aperture and each configuration. Figure 2 shows the configuration for each side that has the maximum deviation from the average value of Table 4. The small aperture observations using the PRISM were not made. However, early observations of G191B2B on the red side in 90 Oct. suggest that the averages of the ratios in Table 4 for the high dispersion gratings is appropriate for each small aperture on the blue and red side, respectively.

b. Data Distribution

The S^{-1} curves are available in digital form on the STSCIC VAX cluster at the Space Telescope Science Institute (STScI). STSDAS compatable GEIS files can be found in DISK$REFERENCE:[CDBSDATA.REFER.YREF] in the files with extensions of '.r2h' and '.r2d'. If direct access to this system is not available, then contact the User Support Branch at the STScI.

IV. Comparison and Error Analysis

By comparing individual S^{-1} curves for a given configuration an estimate of the internal uncertainty can be derived. The internal scatter of the S^{-1} curves about the average is roughly 5% in the 1991.4 to 1992.0 period. About 3% of this scatter is due to focus changes that were unaccounted for at the time of the 1992 Mar 30 delivery to CDBS. On the blue side, the scatter is dominated by changes with time in the sensitivity (see section V).

A check on internal consistency is afforded by comparing fluxes in wavelength regions where the spectral range for two dispersers overlaps. These flux distributions are derived from the countrates in the 4.3″ aperture and the average calibrations of Figure 1. A typical overlap plot is shown in Figure 3.

As another check on internal consistency, we compared the fluxes derived from the input observations to the published fluxes for the star observed. For epochs close to 1991.7, the FOS fluxes track the published fluxes to better than 2%.

Comparisons of the Oke (1990) fluxes to FOS fluxes for BD+33D2642 show a systematic offset longward of 3200Å. Therefore, observations of BD+33D2642 are not included in the 1991.4-1992.0 average calibrations. This offset for BD+33D2642 in the published flux values can also be seen in the trend analysis (see next section and Fig. 4).

V. Trend Analysis and Work in Progress

Figure 4 shows the trend of FOS sensitivity with time for each configuration observed through the 4.3″ aperture within three broad wavelength bands with respect to the 1992 Mar 30 delivery. A correction to the observed sensitivity is included in Figure 4 for the effect of focus change. The blue side exhibits a steady downward trend in sensitivity of about 10% per year. The red side shows a constant sensitivity to within about 5% over the same time period with the exception of the G190H, and G160L dispersers, which exhibit some downward trend in the 1800 to 2100Å range.

A recent model using the FOS point spread function of the light loss as a function of distance in the y direction from the optimum ybase position shows that the maximum predicted GIM shift in the y direction of 65 ybase units on the red side produces a light loss of 5%. This model revealed that with the current spacing between ysteps of 10.67 ybase units, the light loss for a given absolute photometry observation using three ysteps could be greater than 0.5%. For absolute photometry observations after 1991.4 the spacing between ysteps will be 21.33 to insure a maximum light loss of less than 0.5%. The variation among S^{-1} curves for a given configuration on the red side, after removing a linear trend in time, is about $\pm 3\%$ in the worst cases (G270H, and G190H). For the other high dispersion gratings it is typically $\pm 1\%$. An experiment was performed to see if the light loss model could be used to reduce this variation. The results show that in the worst cases the variation is reduced from $\pm 3\%$ to $\pm 2.9\%$ and in the other cases the variation is not significantly changed. We conclude that this correction for the loss of light is insignificant. On the blue side, the variation among S^{-1} curves for a given disperser, after removing a linear trend in time, is also about $\pm 3\%$ in the worst case (G130H), and for the other cases is typically $\pm 2\%$. The light loss model produces an even smaller correction for the blue side because the GIM is roughly a factor of four smaller in magnitude.

A set of S^{-1} curves with better accuracy than those presented here will be derived by accounting for the focus changes in the averaging of multiple curves, and by accounting for the sensitivity trends where necessary. The S^{-1} curves for the paired apertures will also be calculated for future deliveries.

VI. References

Anderson, S. F. 1992, FOS Instrument Science Report CAL/FOS-075.

Bohlin, R. C., Harris, A. W., Holm, A. V., Gry, C. 1990, *Ap. J. Suppl.*, **73**, 413.

Hartig, G., Lindler, D., Beaver, E., Junkkarinen, V., and Lyons, R. 1992, FOS Instrument Science Report, in preparation.

Keyes, A. 1992, private communication.

Lindler, D., and Bohlin, R. 1988, FOS Instrument Science Report CAL/FOS-045.

Oke, J. B. 1990, *Astron. J.*, **99**, 1621.

TABLE 1.

FOS ABSOLUTE CALIBRATION OBSERVATIONS

ROOTNAME	PROPOSAL	DIGICON	DISP.	APER	STAR NAME	OBS. DATE
GROUP 1: USED IN 1992 MAR 30 DELIVERY						
Y0K40304T	3106	BLUE	H13	A-1	BD+75D325	1991.40
Y0K40307T	3106	BLUE	H40	A-1	BD+75D325	1991.40
Y0K40308T	3106	BLUE	L15	A-1	BD+75D325	1991.40
Y0K4030AT	3106	BLUE	H27	A-1	BD+75D325	1991.40
Y0K4030DT	3106	BLUE	H19	A-1	BD+75D325	1991.40
Y0K40204T	3106	RED	H78	A-1	BD+75D325	1991.40
Y0K40207T	3106	RED	H27	A-1	BD+75D325	1991.40
Y0K40208T	3106	RED	H19	A-1	BD+75D325	1991.40
Y0K4020BT	3106	RED	H57	A-1	BD+75D325	1991.40
Y0K4020CT	3106	RED	H40	A-1	BD+75D325	1991.40
Y0K4020FT	3106	RED	L15	A-1	BD+75D325	1991.40
Y0K4020GT	3106	RED	L65	A-1	BD+75D325	1991.40
Y0K4510ZT	3106	BLUE	H13	A-1	BD+75D325	1991.43
Y0K45112T	3106	BLUE	H40	A-1	BD+75D325	1991.43
Y0K45113T	3106	BLUE	L15	A-1	BD+75D325	1991.43
Y0K45115T	3106	BLUE	H27	A-1	BD+75D325	1991.43
Y0K45118T	3106	BLUE	H19	A-1	BD+75D325	1991.43
Y0K45804T	3106	BLUE	H13	A-1	HZ-44	1991.48
Y0K45807T	3106	BLUE	H40	A-1	HZ-44	1991.48
Y0K45808T	3106	BLUE	L15	A-1	HZ-44	1991.48
Y0K4580BT	3106	BLUE	PRI	A-1	HZ-44	1991.48
Y0K4580CT	3106	BLUE	H27	A-1	HZ-44	1991.48
Y0K4580FT	3106	BLUE	H19	A-1	HZ-44	1991.48

Y0O60105T	2823	RED	H27	A-1	BD+28D4211	1991.54
Y0O60106T	2823	RED	H19	A-1	BD+28D4211	1991.54
Y0O60109T	2823	RED	H57	A-1	BD+28D4211	1991.54
Y0O6010AT	2823	RED	H40	A-1	BD+28D4211	1991.54
Y0O6010DT	2823	RED	L15	A-1	BD+28D4211	1991.54
Y0O6010ET	2823	RED	L65	A-1	BD+28D4211	1991.54
Y0O6010HT	2823	RED	PRI	A-1	BD+28D4211	1991.54
Y0K40504T	3106	BLUE	H13	A-1	BD+75D325	1991.56
Y0K40507T	3106	BLUE	H40	A-1	BD+75D325	1991.56
Y0K40508T	3106	BLUE	L15	A-1	BD+75D325	1991.56
Y0K4050AT	3106	BLUE	H27	A-1	BD+75D325	1991.56
Y0K4050DT	3106	BLUE	H19	A-1	BD+75D325	1991.56
Y0K45504T	3106	BLUE	H13	A-1	BD+75D325	1991.73
Y0K45507T	3106	BLUE	H40	A-1	BD+75D325	1991.73
Y0K45508T	3106	BLUE	L15	A-1	BD+75D325	1991.73
Y0K4550AT	3106	BLUE	H27	A-1	BD+75D325	1991.73
Y0K4550DT	3106	BLUE	H19	A-1	BD+75D325	1991.73
Y0O65105T	2823	RED	H27	A-1	BD+28D4211	1991.74
Y0O65106T	2823	RED	H19	A-1	BD+28D4211	1991.74
Y0O65109T	2823	RED	H57	A-1	BD+28D4211	1991.74
Y0O6510AT	2823	RED	H40	A-1	BD+28D4211	1991.74
Y0O6510DT	2823	RED	L15	A-1	BD+28D4211	1991.74
Y0O6510ET	2823	RED	L65	A-1	BD+28D4211	1991.74
Y0O6510HT	2823	RED	PRI	A-1	BD+28D4211	1991.74
Y0K40404T	3106	RED	H78	A-1	BD+75D325	1991.81
Y0K40407T	3106	RED	H27	A-1	BD+75D325	1991.81
Y0K40408T	3106	RED	H19	A-1	BD+75D325	1991.81
Y0K4040BT	3106	RED	H57	A-1	BD+75D325	1991.81
Y0K4040CT	3106	RED	H40	A-1	BD+75D325	1991.81
Y0K4040FT	3106	RED	L15	A-1	BD+75D325	1991.81
Y0K4040GT	3106	RED	L65	A-1	BD+75D325	1991.81
Y0K4561BT	3106	RED	H78	A-1	BD+75D325	1991.96
Y0K4561ET	3106	RED	H27	A-1	BD+75D325	1991.96
Y0K4561FT	3106	RED	H19	A-1	BD+75D325	1991.96
Y0K4561IT	3106	RED	H57	A-1	BD+75D325	1991.96
Y0K4561JT	3106	RED	H40	A-1	BD+75D325	1991.96
Y0K4561MT	3106	RED	L15	A-1	BD+75D325	1991.96
Y0K4561NT	3106	RED	L65	A-1	BD+75D325	1991.96

GROUP 2: FAILED TARGET ACQUISITION

Y0K45704T	3106	BLUE	H13	A-1	BD+33D2642	1991.47
Y0K45707T	3106	BLUE	H40	A-1	BD+33D2642	1991.47
Y0K45708T	3106	BLUE	L15	A-1	BD+33D2642	1991.47
Y0K4570BT	3106	BLUE	PRI	A-1	BD+33D2642	1991.47
Y0K4570CT	3106	BLUE	H27	A-1	BD+33D2642	1991.47
Y0K4570FT	3106	BLUE	H19	A-1	BD+33D2642	1991.47

GROUP 3: LARGE SYSTEMATIC ERROR IN PUBLISHED FLUX FOR BD+33D2642

Y0K46704T	3106	BLUE	H13	A-1	BD+33D2642	1991.66
Y0K46707T	3106	BLUE	H40	A-1	BD+33D2642	1991.66
Y0K46708T	3106	BLUE	L15	A-1	BD+33D2642	1991.66
Y0K4670BT	3106	BLUE	PRI	A-1	BD+33D2642	1991.66
Y0K4670CT	3106	BLUE	H27	A-1	BD+33D2642	1991.66
Y0K4670FT	3106	BLUE	H19	A-1	BD+33D2642	1991.66

GROUP 4: LARGE SCATTER DUE TO FOCUS CHANGES

Y0ER0I04T	1320	RED	H78	A-1	BD+33D2642	1990.91
Y0ER0I07T	1320	RED	H27	A-1	BD+33D2642	1990.91
Y0ER0I08T	1320	RED	H19	A-1	BD+33D2642	1990.91
Y0ER0I0BT	1320	RED	H57	A-1	BD+33D2642	1990.91
Y0ER0I0CT	1320	RED	H40	A-1	BD+33D2642	1990.91
Y0ER0I0FT	1320	RED	L15	A-1	BD+33D2642	1990.91
Y0ER0I0GT	1320	RED	L65	A-1	BD+33D2642	1990.91
Y0ER0I0JT	1320	RED	PRI	A-1	BD+33D2642	1990.91
Y0ER0C04T	1320	RED	H78	A-1	BD+28D4211	1990.92
Y0ER0C07T	1320	RED	H27	A-1	BD+28D4211	1990.92
Y0ER0C08T	1320	RED	H19	A-1	BD+28D4211	1990.92
Y0ER0C0BT	1320	RED	H57	A-1	BD+28D4211	1990.92
Y0ER0C0CT	1320	RED	H40	A-1	BD+28D4211	1990.92
Y0ER0C0FT	1320	RED	L15	A-1	BD+28D4211	1990.92
Y0ER0C0GT	1320	RED	L65	A-1	BD+28D4211	1990.92
Y0ER0C0JT	1320	RED	PRI	A-1	BD+28D4211	1990.92
Y0ER0E04T	1320	BLUE	H13	A-1	BD+33D2642	1991.03
Y0ER0E07T	1320	BLUE	H40	A-1	BD+33D2642	1991.03
Y0ER0E08T	1320	BLUE	L15	A-1	BD+33D2642	1991.03
Y0ER0E0BT	1320	BLUE	PRI	A-1	BD+33D2642	1991.03
Y0ER0E0CT	1320	BLUE	H27	A-1	BD+33D2642	1991.03
Y0ER0E0FT	1320	BLUE	H19	A-1	BD+33D2642	1991.03
Y0ER0F04T	1320	RED	H78	A-1	BD+33D2642	1991.03
Y0ER0F07T	1320	RED	H27	A-1	BD+33D2642	1991.03
Y0ER0F08T	1320	RED	H19	A-1	BD+33D2642	1991.03
Y0ER0F0BT	1320	RED	H57	A-1	BD+33D2642	1991.03
Y0ER0F0CT	1320	RED	H40	A-1	BD+33D2642	1991.03
Y0ER0F0FT	1320	RED	L15	A-1	BD+33D2642	1991.03
Y0ER0F0GT	1320	RED	L65	A-1	BD+33D2642	1991.03
Y0ER0F0JT	1320	RED	PRI	A-1	BD+33D2642	1991.03
Y0ER0204T	1320	BLUE	H13	A-1	BD+75D325	1991.03
Y0ER0207T	1320	BLUE	H40	A-1	BD+75D325	1991.03
Y0ER0208T	1320	BLUE	L15	A-1	BD+75D325	1991.03
Y0ER020BT	1320	BLUE	PRI	A-1	BD+75D325	1991.03
Y0ER020CT	1320	BLUE	H27	A-1	BD+75D325	1991.03
Y0ER020FT	1320	BLUE	H19	A-1	BD+75D325	1991.03
Y0ER0K04T	1320	BLUE	H13	A-1	HZ-44	1991.03
Y0ER0K07T	1320	BLUE	H40	A-1	HZ-44	1991.03
Y0ER0K08T	1320	BLUE	L15	A-1	HZ-44	1991.03
Y0ER0K0BT	1320	BLUE	PRI	A-1	HZ-44	1991.03
Y0ER0K0CT	1320	BLUE	H27	A-1	HZ-44	1991.03
Y0ER0K0FT	1320	BLUE	H19	A-1	HZ-44	1991.03
Y0ER0L04T	1320	RED	H78	A-1	HZ-44	1991.03
Y0ER0L07T	1320	RED	H27	A-1	HZ-44	1991.03
Y0ER0L08T	1320	RED	H19	A-1	HZ-44	1991.04
Y0ER0L0BT	1320	RED	H57	A-1	HZ-44	1991.04
Y0ER0L0CT	1320	RED	H40	A-1	HZ-44	1991.04
Y0ER0L0FT	1320	RED	L15	A-1	HZ-44	1991.04
Y0ER0L0GT	1320	RED	L65	A-1	HZ-44	1991.04
Y0ER0L0JT	1320	RED	PRI	A-1	HZ-44	1991.04

GROUP 5: RECENT OBSERVATIONS NOT USED FOR 1992 MAR 30 DELIVERY

Y0TM0104T	3975	RED	H27	A-1	WD0501+527	1992.01
Y0TM0105T	3975	RED	H19	A-1	WD0501+527	1992.01
Y0TM0106T	3975	RED	L15	A-1	WD0501+527	1992.01
Y0TM0204T	3975	RED	H27	A-1	WD0501+527	1992.07
Y0TM0205T	3975	RED	H19	A-1	WD0501+527	1992.07
Y0TM0206T	3975	RED	L15	A-1	WD0501+527	1992.07
Y0TM0304T	3975	RED	H27	A-1	WD0501+527	1992.15
Y0TM0305T	3975	RED	H19	A-1	WD0501+527	1992.15
Y0TM0306T	3975	RED	L15	A-1	WD0501+527	1992.15
Y0VH0507T	2821	BLUE	PRI	A-1	WD0501+527	1992.18
Y0VH050AT	2821	BLUE	H27	A-1	WD0501+527	1992.18
Y0VH050JT	2821	BLUE	H19	A-1	WD0501+527	1992.18
Y0VH050MT	2821	BLUE	H13	A-1	WD0501+527	1992.18
Y0VH050ST	2821	BLUE	H40	A-1	WD0501+527	1992.18
Y0VH050VT	2821	BLUE	L15	A-1	WD0501+527	1992.18

GROUP 6: APERTURE TRANSMISSION FOR SINGLE APERTURES

Y0K45105T	3106	BLUE	H13	B-2	BD+75D325	1991.43
Y0K45108T	3106	BLUE	H40	B-2	BD+75D325	1991.43
Y0K45109T	3106	BLUE	L15	B-2	BD+75D325	1991.43
Y0K4510BT	3106	BLUE	H27	B-2	BD+75D325	1991.43
Y0K4510ET	3106	BLUE	H19	B-2	BD+75D325	1991.43
Y0K4510FT	3106	BLUE	H13	B-1	BD+75D325	1991.43
Y0K4510IT	3106	BLUE	H40	B-1	BD+75D325	1991.43
Y0K4510JT	3106	BLUE	L15	B-1	BD+75D325	1991.43
Y0K4510LT	3106	BLUE	H27	B-1	BD+75D325	1991.43
Y0K4510OT	3106	BLUE	H19	B-1	BD+75D325	1991.43
Y0K4510PT	3106	BLUE	H13	B-3	BD+75D325	1991.43
Y0K4510ST	3106	BLUE	H40	B-3	BD+75D325	1991.43
Y0K4510TT	3106	BLUE	L15	B-3	BD+75D325	1991.43
Y0K4510VT	3106	BLUE	H27	B-3	BD+75D325	1991.43
Y0K4510YT	3106	BLUE	H19	B-3	BD+75D325	1991.43
Y0K4511AT	3106	BLUE	H13	C-2	BD+75D325	1991.43
Y0K4511DT	3106	BLUE	H40	C-2	BD+75D325	1991.43
Y0K4511ET	3106	BLUE	L15	C-2	BD+75D325	1991.43
Y0K4511GT	3106	BLUE	H27	C-2	BD+75D325	1991.43
Y0K4511JT	3106	BLUE	H19	C-2	BD+75D325	1991.43
Y0K45605T	3106	RED	H78	B-2	BD+75D325	1991.96
Y0K45608T	3106	RED	H27	B-2	BD+75D325	1991.96
Y0K45609T	3106	RED	H19	B-2	BD+75D325	1991.96
Y0K4560CT	3106	RED	H57	B-2	BD+75D325	1991.96
Y0K4560DT	3106	RED	H40	B-2	BD+75D325	1991.96
Y0K4560GT	3106	RED	L15	B-2	BD+75D325	1991.96
Y0K4560HT	3106	RED	L65	B-2	BD+75D325	1991.96
Y0K4560JT	3106	RED	H78	B-1	BD+75D325	1991.96
Y0K4560MT	3106	RED	H27	B-1	BD+75D325	1991.96
Y0K4560NT	3106	RED	H19	B-1	BD+75D325	1991.96
Y0K4560QT	3106	RED	H57	B-1	BD+75D325	1991.96
Y0K4560RT	3106	RED	H40	B-1	BD+75D325	1991.96
Y0K4560UT	3106	RED	L15	B-1	BD+75D325	1991.96
Y0K4560VT	3106	RED	L65	B-1	BD+75D325	1991.96
Y0K4560XT	3106	RED	H78	B-3	BD+75D325	1991.96
Y0K45610T	3106	RED	H27	B-3	BD+75D325	1991.96
Y0K45611T	3106	RED	H19	B-3	BD+75D325	1991.96
Y0K45614T	3106	RED	H57	B-3	BD+75D325	1991.96
Y0K45615T	3106	RED	H40	B-3	BD+75D325	1991.96
Y0K45618T	3106	RED	L15	B-3	BD+75D325	1991.96
Y0K45619T	3106	RED	L65	B-3	BD+75D325	1991.96
Y0K4561QT	3106	RED	H78	C-2	BD+75D325	1991.96
Y0K4561TT	3106	RED	H27	C-2	BD+75D325	1991.96
Y0K4561UT	3106	RED	H19	C-2	BD+75D325	1991.96
Y0K4561XT	3106	RED	H57	C-2	BD+75D325	1991.96
Y0K4561YT	3106	RED	H40	C-2	BD+75D325	1991.96
Y0K45621T	3106	RED	L15	C-2	BD+75D325	1991.96
Y0K45622T	3106	RED	L65	C-2	BD+75D325	1991.96

GROUP 7: APERTURE TRANSMISSION FOR PAIRED APERTURES

Y0O6510KT	2823	RED	H27	A-3	BD+28D4211	1991.74
Y0O6510LT	2823	RED	H19	A-3	BD+28D4211	1991.74
Y0O6510OT	2823	RED	H57	A-3	BD+28D4211	1991.74
Y0O6510PT	2823	RED	H40	A-3	BD+28D4211	1991.74
Y0O6510ST	2823	RED	H27	A-2	BD+28D4211	1991.74
Y0O6510TT	2823	RED	H19	A-2	BD+28D4211	1991.74
Y0O6510WT	2823	RED	H57	A-2	BD+28D4211	1991.74
Y0O6510XT	2823	RED	H40	A-2	BD+28D4211	1991.74
Y0O65110T	2823	RED	H27	C-1	BD+28D4211	1991.74
Y0O65111T	2823	RED	H19	C-1	BD+28D4211	1991.74
Y0O65114T	2823	RED	H57	C-1	BD+28D4211	1991.74
Y0O65115T	2823	RED	H40	C-1	BD+28D4211	1991.74
Y0O65119T	2823	RED	H27	A-3	BD+28D4211	1991.74
Y0O6511AT	2823	RED	H19	A-3	BD+28D4211	1991.74
Y0O6511DT	2823	RED	H57	A-3	BD+28D4211	1991.74
Y0O6511ET	2823	RED	H40	A-3	BD+28D4211	1991.74
Y0O6511HT	2823	RED	H27	A-2	BD+28D4211	1991.74
Y0O6511IT	2823	RED	H19	A-2	BD+28D4211	1991.74
Y0O6511LT	2823	RED	H57	A-2	BD+28D4211	1991.74
Y0O6511MT	2823	RED	H40	A-2	BD+28D4211	1991.74
Y0O6511PT	2823	RED	H27	C-1	BD+28D4211	1991.74
Y0O6511QT	2823	RED	H19	C-1	BD+28D4211	1991.74
Y0O6511TT	2823	RED	H57	C-1	BD+28D4211	1991.74
Y0O6511UT	2823	RED	H40	C-1	BD+28D4211	1991.74

TABLE 2.
FOS DETECTOR-DISPERSER COMBINATIONS

BLUE DIGICON	RED DIGICON	NODES
G130H (H13)		12 *
G190H (H19)	G190H (H19)	21 *
G270H (H27)	G270H (H27)	7
G400H (H40)	G400H (H40)	10
	G570H (H57)	10
	G780H (H78)	10
G160L (L15)	G160L (L15)	13 (25) *
	G650L (L65)	17 *
PRISM (PRI)	PRISM (PRI)	28 *

TABLE 3.
FOS ENTRANCE APERTURES

DESIGNATION	SIZE(")	SHAPE	SINGLE/PAIRED
A-1	4.30	SQUARE	SINGLE
B-1	0.50	CIRCULAR	SINGLE
B-2	0.30	CIRCULAR	SINGLE
B-3	1.00	CIRCULAR	SINGLE
C-2	0.25 X 2.00	SLIT	SINGLE
A-2	0.50	SQUARE	PAIRED
A-3	0.25	SQUARE	PAIRED
A-4	0.10	SQUARE	PAIRED
C-1	1.00	SQUARE	PAIRED

TABLE 4.
SUMMARY OF APERTURE THROUGHPUT RATIOS

DETEC.	DISP.	APER.	RATIO
BLUE	H13	B-1	0.39
BLUE	H13	B-2	0.24
BLUE	H13	B-3	0.60
BLUE	H13	C-2	0.37
BLUE	H19	B-1	0.41
BLUE	H19	B-2	0.24
BLUE	H19	B-3	0.61
BLUE	H19	C-2	0.38
BLUE	H27	B-1	0.42
BLUE	H27	B-2	0.25
BLUE	H27	B-3	0.58
BLUE	H27	C-2	0.38
BLUE	H40	B-1	0.42
BLUE	H40	B-2	0.26
BLUE	H40	B-3	0.57
BLUE	H40	C-2	0.38
BLUE	L15	B-1	0.45
BLUE	L15	B-2	0.29
BLUE	L15	B-3	0.66
BLUE	L15	C-2	0.41
RED	H19	B-1	0.43
RED	H19	B-2	0.31
RED	H19	B-3	0.60
RED	H19	C-2	0.41
RED	H27	B-1	0.44
RED	H27	B-2	0.32
RED	H27	B-3	0.59
RED	H27	C-2	0.41
RED	H40	B-1	0.44
RED	H40	B-2	0.32
RED	H40	B-3	0.60
RED	H40	C-2	0.42
RED	H57	B-1	0.44
RED	H57	B-2	0.31
RED	H57	B-3	0.59
RED	H57	C-2	0.41
RED	H78	B-1	0.43
RED	H78	B-2	0.28
RED	H78	B-3	0.58
RED	H78	C-2	0.40
RED	L15	B-1	0.48
RED	L15	B-2	0.29
RED	L15	B-3	0.65
RED	L15	C-2	0.44
RED	L65	B-1	0.49
RED	L65	B-2	0.35
RED	L65	B-3	0.66
RED	L65	C-2	0.44

FIG 1. - a) through n) Inverse sensitivity (S−1) curves as delivered on March 30th, 1992 for each detector-disperser combination. The A-1 curve is the average of the curves generated from the individual observations, while the other single apertures are derived by applying the throughput ratio functions as described in section IIIa.

FIG 2. - a) The aperture ratio data and fits for the circular single apertures with respect to the A-1 aperture as observed with the blue side H13 (G130H) disperser. This configuration shows the maximum error on the blue side of 3% when using the average ratio values from Table 4. The C-2 slit aperture data falls within the scatter for the B-1 aperture and is not plotted.

FIG 2. - b) The aperture ratio data and fits for the circular single apertures with respect to the A-1 aperture as observed with the red side H19 (G190H) disperser. This configuration is fit with a polynomial of order 2 and has a maximum error of 2% when using the average ratio values from Table 4.

FIG 2. - c) The aperture ratio data and fits for the circular single apertures with respect to the A-1 aperture as observed with the red side L15 (G160L) disperser. The need to mask the short wavelength cutoff is evident. This configuration shows the maximum error on the red side of 3% when using the average ratio values from Table 4.

FIG 3. - The FOS fluxes for BD+75D325 from the set of observations taken with the high dispersion gratings on the red side at the epoch 1991.81. The dashes indicate the extent of the wavelength coverage for the H19, H27, H40, H57, and H78 gratings and demark the regions of overlap. The fluxes are multiplied by the function $(\text{wavelength}/10000.)^{3.5}$, with wavelength in Angstroms, to derive the normalized flux distribution. The fluxes in the overlap regions agree to better than 2%. The broad feature near 2000Å is due to the time variable response in that range.

FIG 4. - a) through n) The sensitivity change as a function of time for each configuration observed through the A-1 aperture in three broad wavelength bands with respect to the March 30th, 1992 delivery. Corrections for changes in the observatory focus have been applied. All observations between 1991.40 and 1991.96, except of BD+33D2642, are used for the delivery of March 30th, 1992.

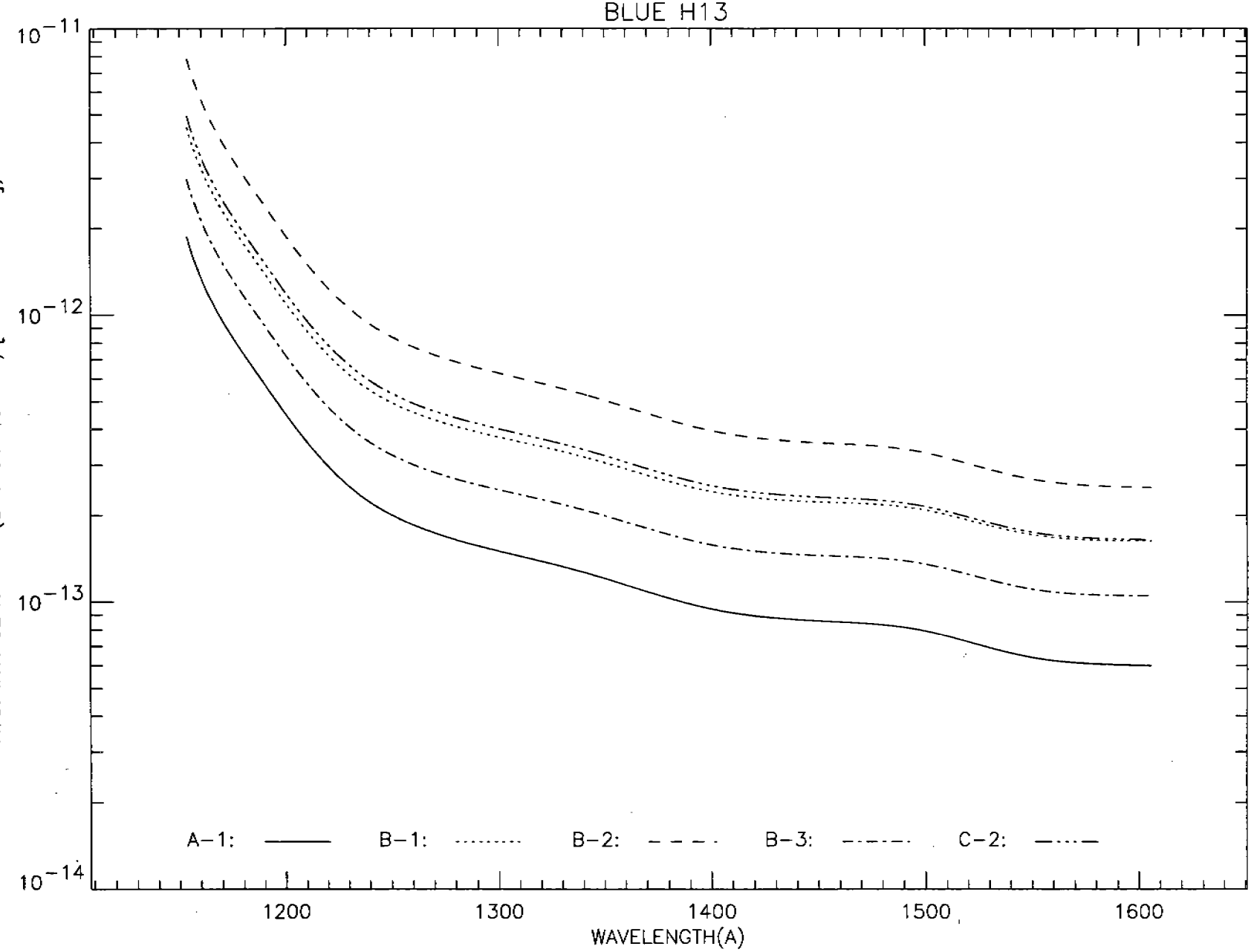
BLUE H13
10^{-11}
10^{-12}
10^{-13}
10^{-14}
AVG. INV. SENSITIVITY(ERG CM^{-2} S^{-1} A^{-1}/[CT S^{-1} DIODE^{-1}])
CAL/FOS-077-18
A-1:
B-1:
B-2:
B-3:
C-2:
1200
1300
1400
1500
1600
WAVELENGTH(A)

Figure 1a

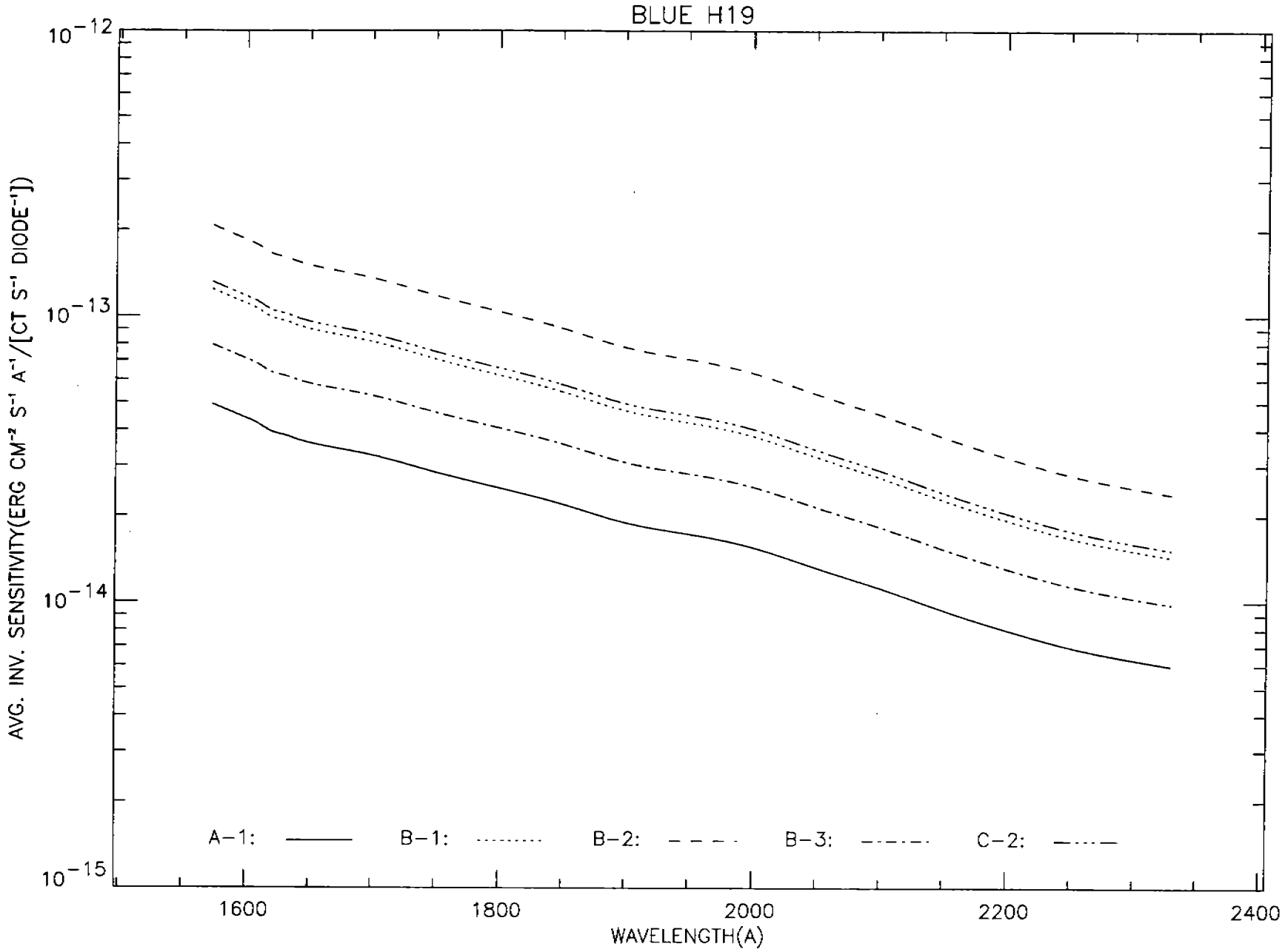

CAL/FOS-077-19

Figure 1b

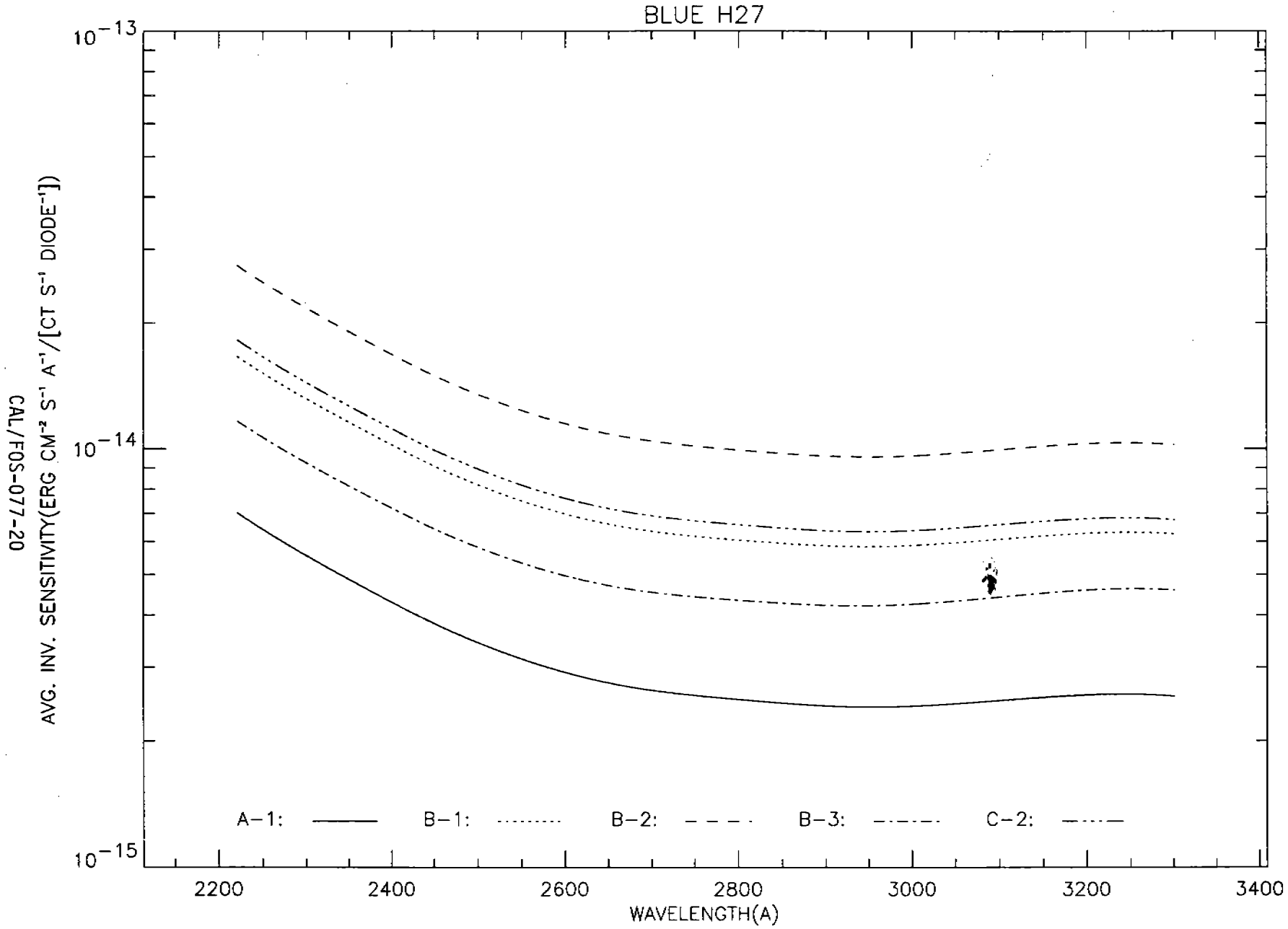
BLUE H27
10^{-13}
10^{-14}
10^{-15}
AVG. INV. SENSITIVITY(ERG CM^{-2} S^{-1} A^{-1}/[CT S^{-1} DIODE^{-1}])
CAL/FOS-077-20
A-1:
B-1:
B-2:
B-3:
C-2:
2200
2400
2600
2800
3000
3200
3400
WAVELENGTH(A)

Figure 1c

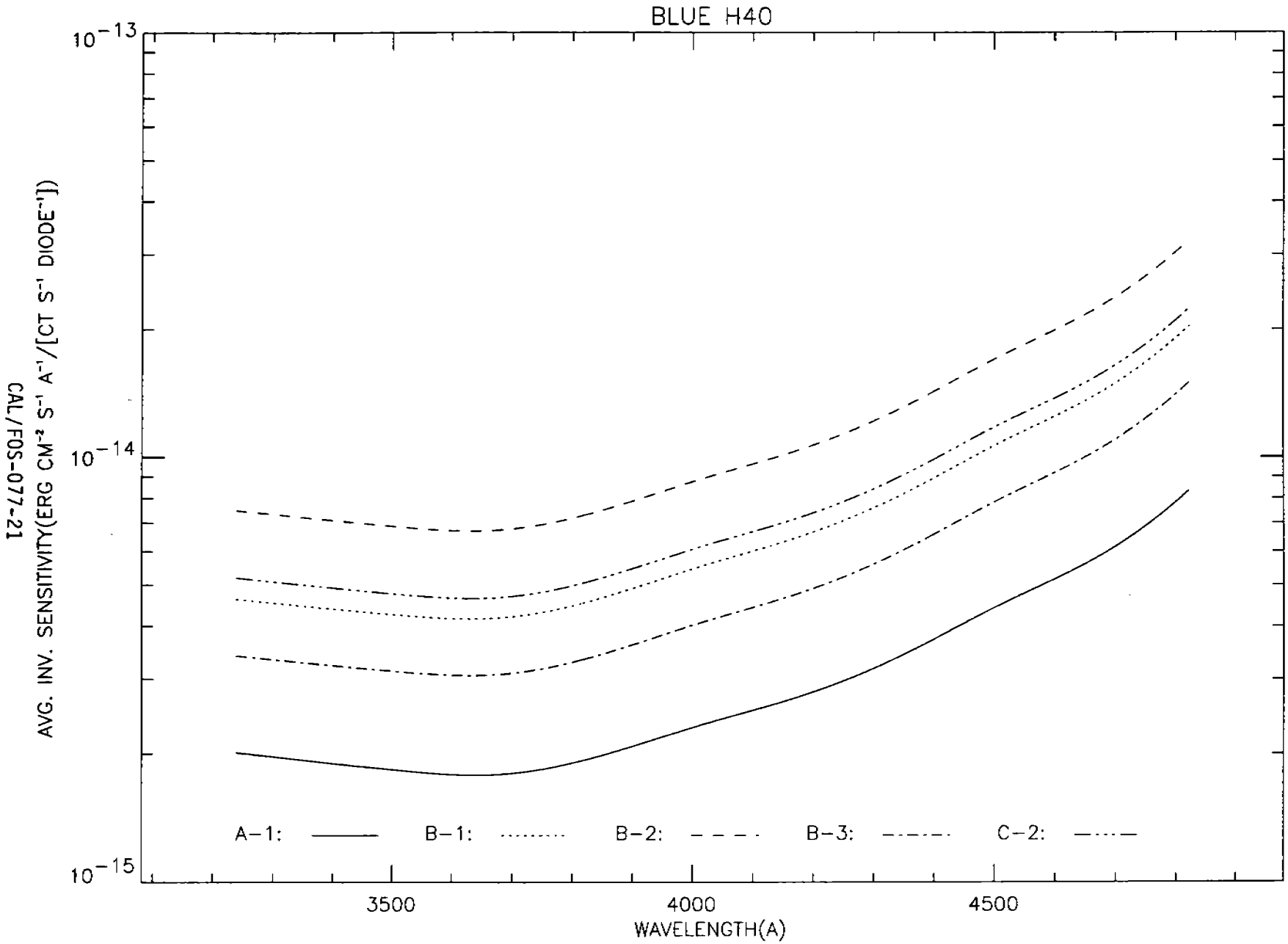
BLUE H40
10^{-13}
10^{-14}
10^{-15}
AVG. INV. SENSITIVITY(ERG CM^{-2} S^{-1} A^{-1}/[CT S^{-1} DIODE^{-1}])
CAL/FOS-077-21
A-1:
B-1:
B-2:
B-3:
C-2:
3500
4000
4500
WAVELENGTH(A)

Figure 1d

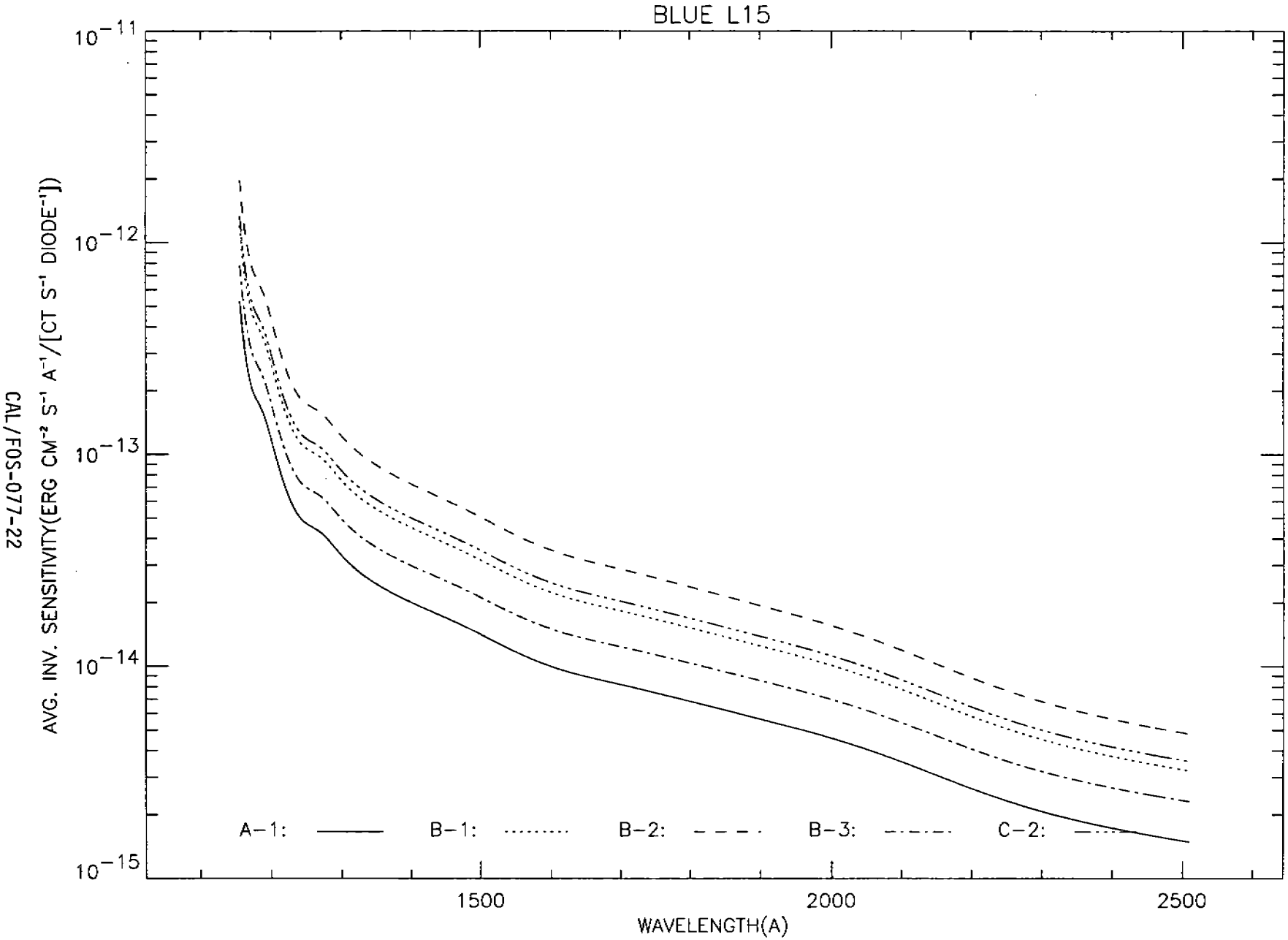
BLUE L15
AVG. INV. SENSITIVITY(ERG CM⁻² S⁻¹ A⁻¹/[CT S⁻¹ DIODE⁻¹])
CAL/FOS-077-22
10⁻¹¹
10⁻¹²
10⁻¹³
10⁻¹⁴
10⁻¹⁵
1500
2000
2500
WAVELENGTH(A)
A-1:
B-1:
B-2:
B-3:
C-2:

Figure 1e

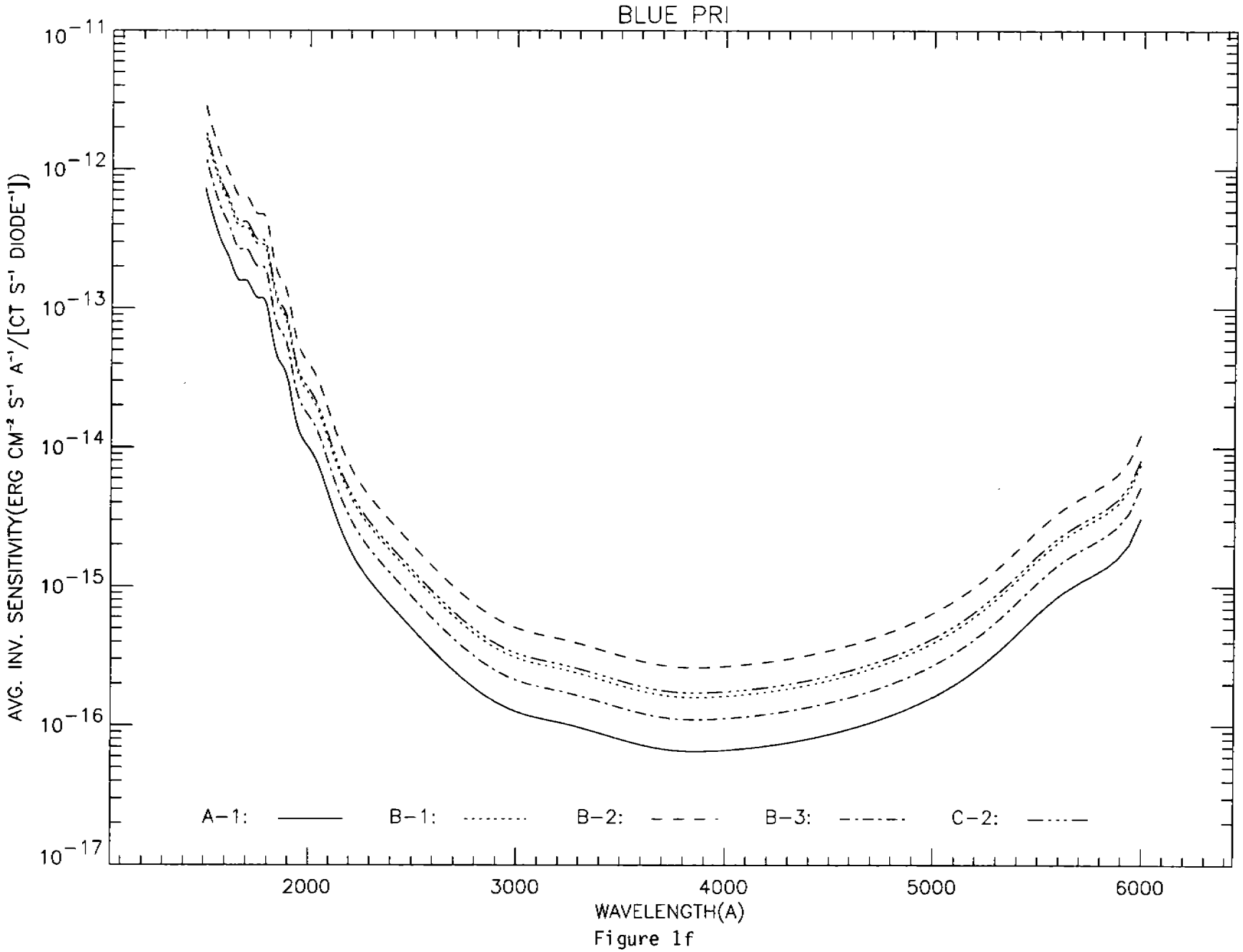

CAL/FOS-077-23

Figure 1f

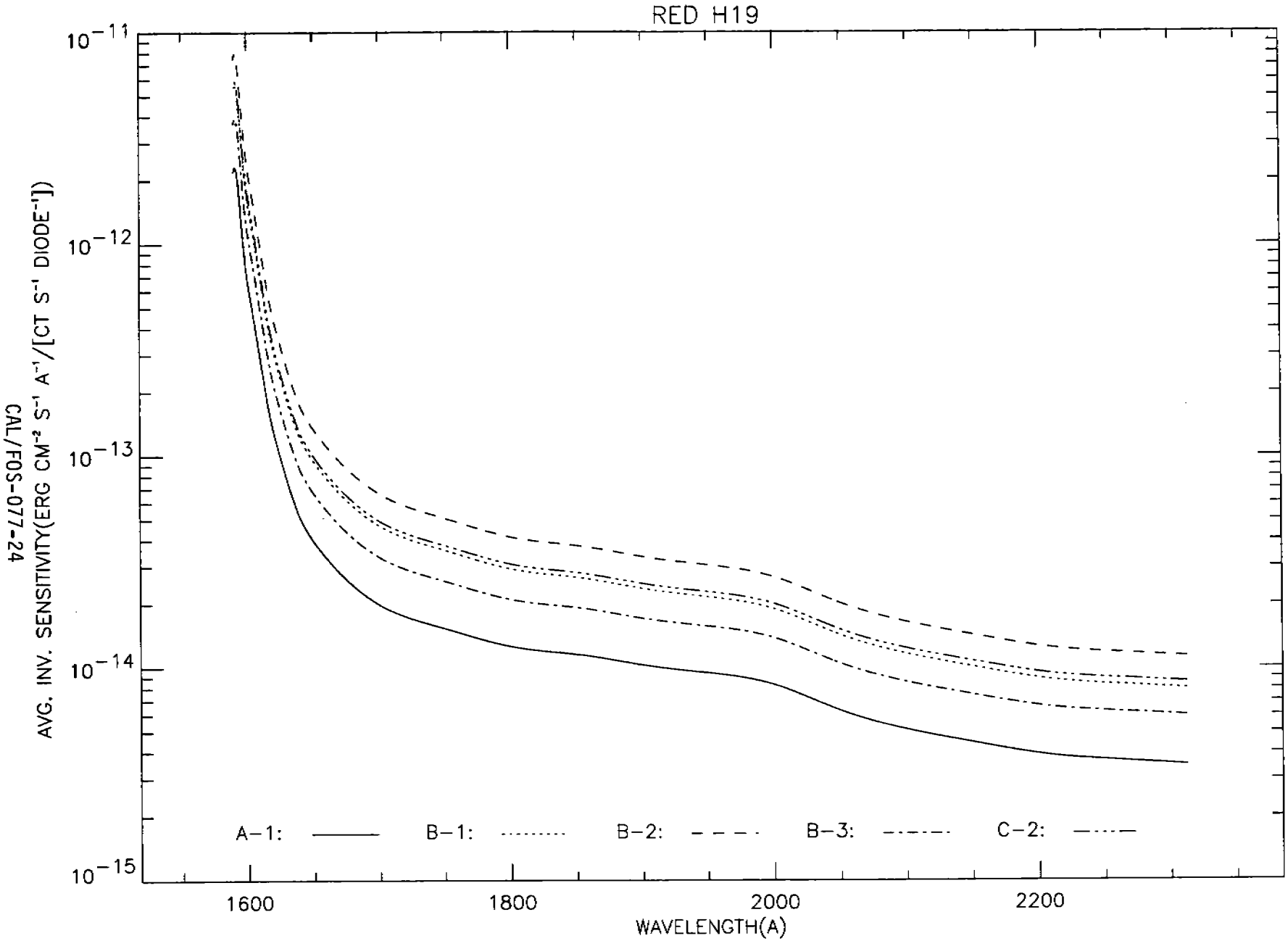
RED H19
AVG. INV. SENSITIVITY(ERG CM⁻² S⁻¹ A⁻¹/[CT S⁻¹ DIODE⁻¹])
CAL/FOS-077-24
10⁻¹¹
10⁻¹²
10⁻¹³
10⁻¹⁴
10⁻¹⁵
1600
1800
2000
2200
WAVELENGTH(A)
A-1:
B-1:
B-2:
B-3:
C-2:

Figure 1g

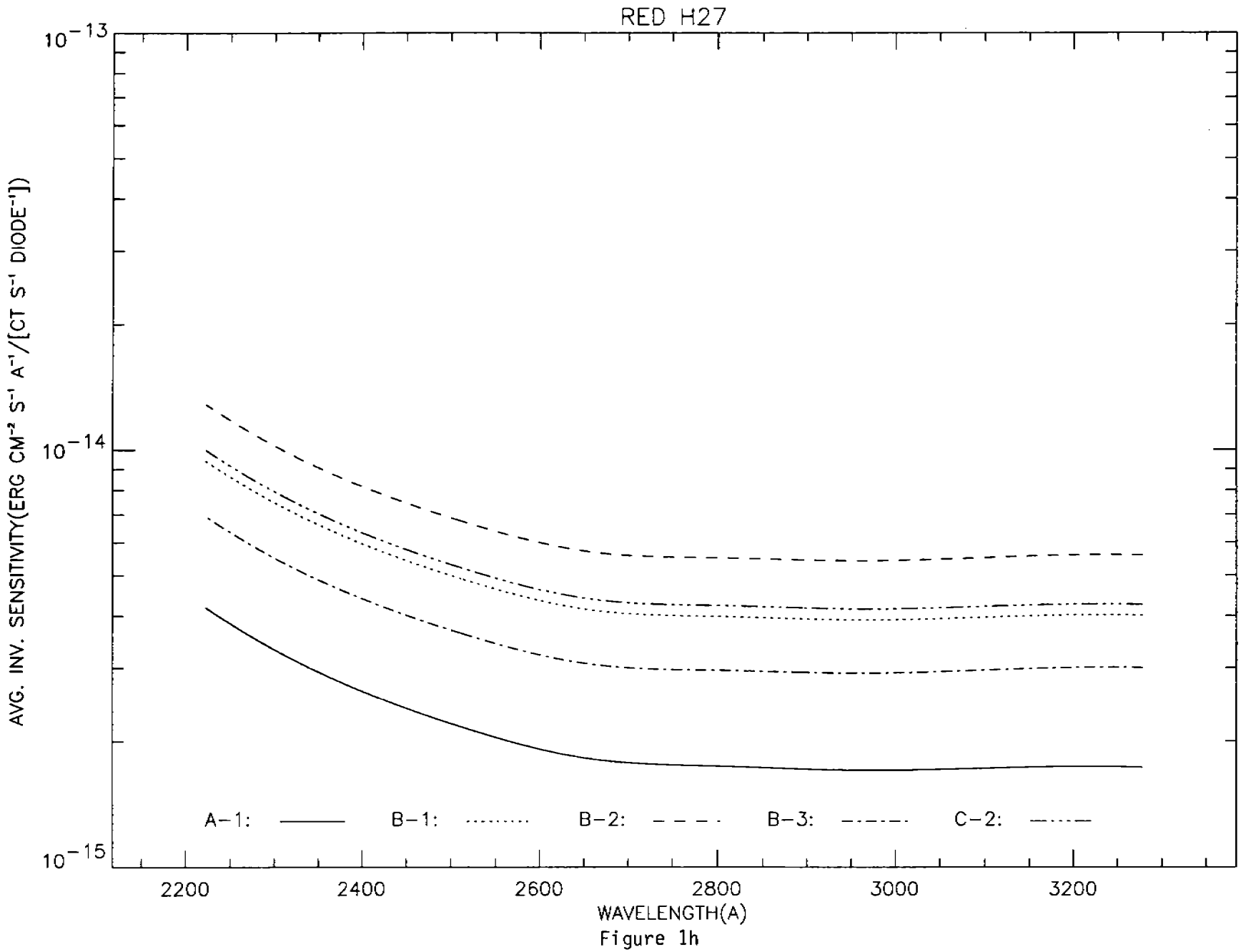
RED H27
10^{-13}
10^{-14}
10^{-15}
AVG. INV. SENSITIVITY(ERG CM^{-2} S^{-1} A^{-1}/[CT S^{-1} DIODE^{-1}])
CAL/FOS-077-25
A-1:
B-1:
B-2:
B-3:
C-2:
2200
2400
2600
2800
3000
3200
WAVELENGTH(A)

Figure 1h

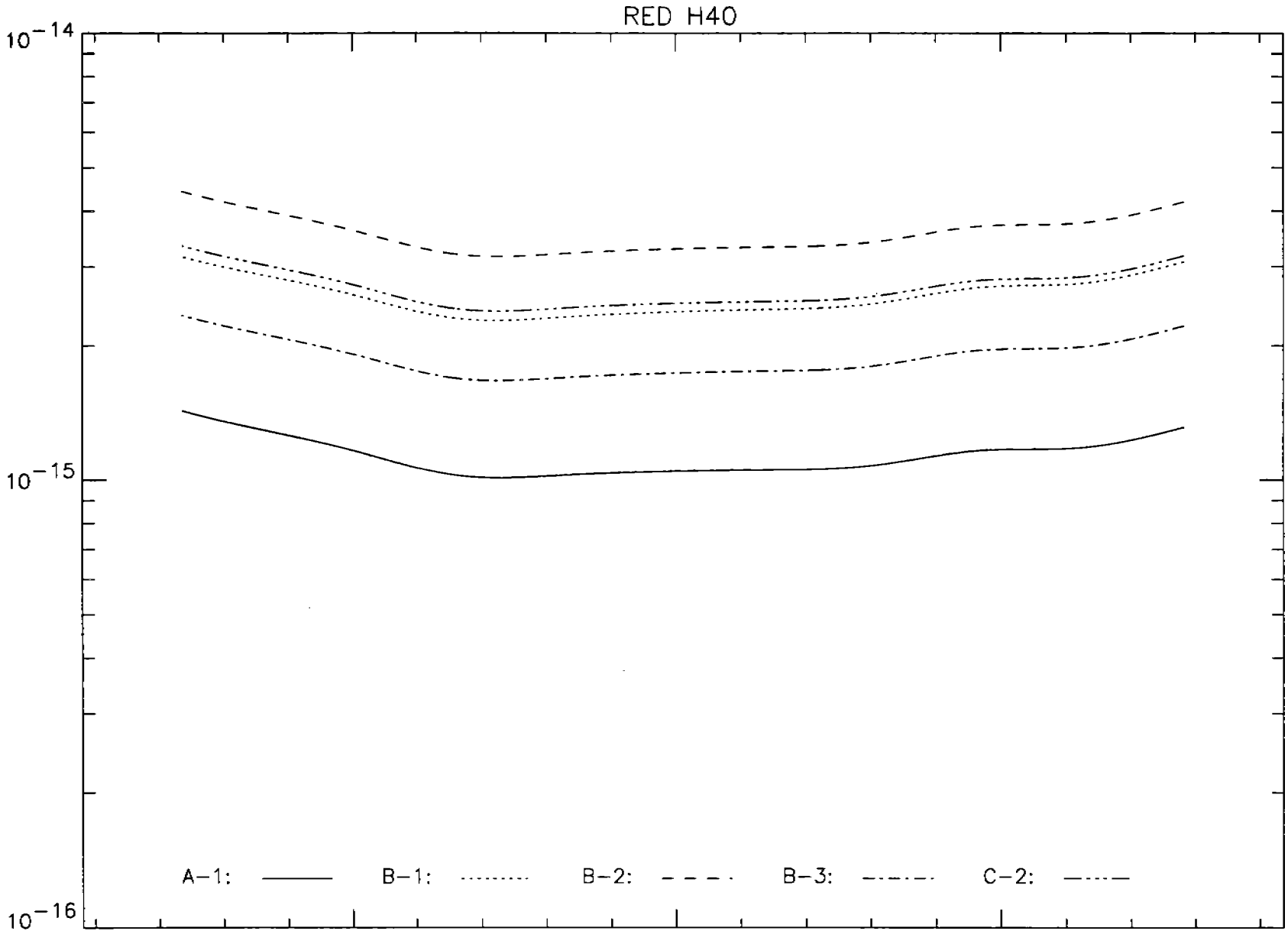
RED H40
10^{-14}
10^{-15}
10^{-16}
AVG. INV. SENSITIVITY(ERG CM^{-2} S^{-1} A^{-1}/[CT S^{-1} DIODE^{-1}])
A-1:
B-1:
B-2:
B-3:
C-2:
3500
4000
4500
WAVELENGTH(A)

Figure 1i

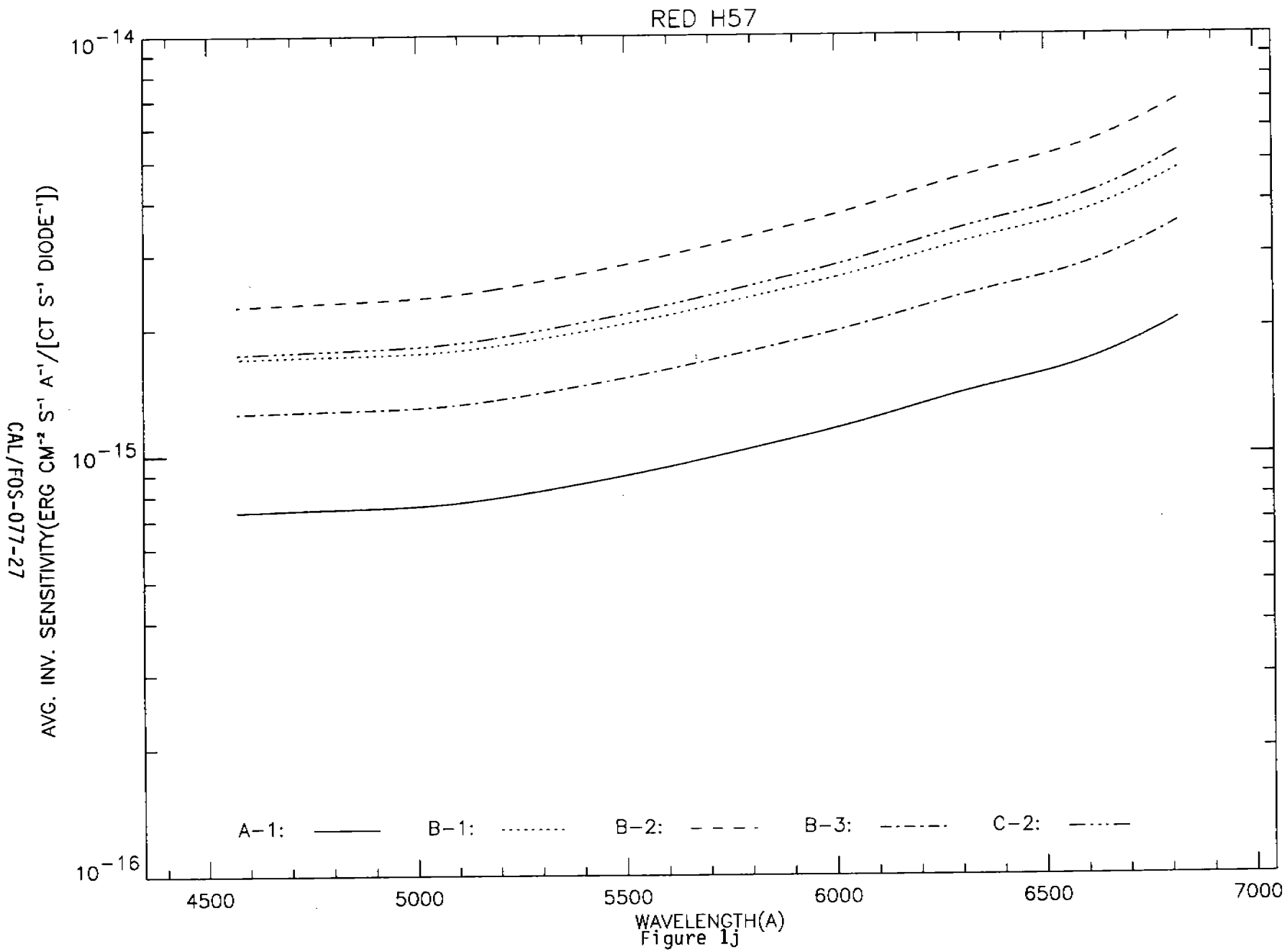
RED H57
10^{-14}
10^{-15}
10^{-16}
AVG. INV. SENSITIVITY(ERG CM^{-2} S^{-1} A^{-1}/[CT S^{-1} DIODE^{-1}])
CAL/FOS-077-27
A-1:
B-1:
B-2:
B-3:
C-2:
4500
5000
5500
6000
6500
7000
WAVELENGTH(A)
Figure 1j

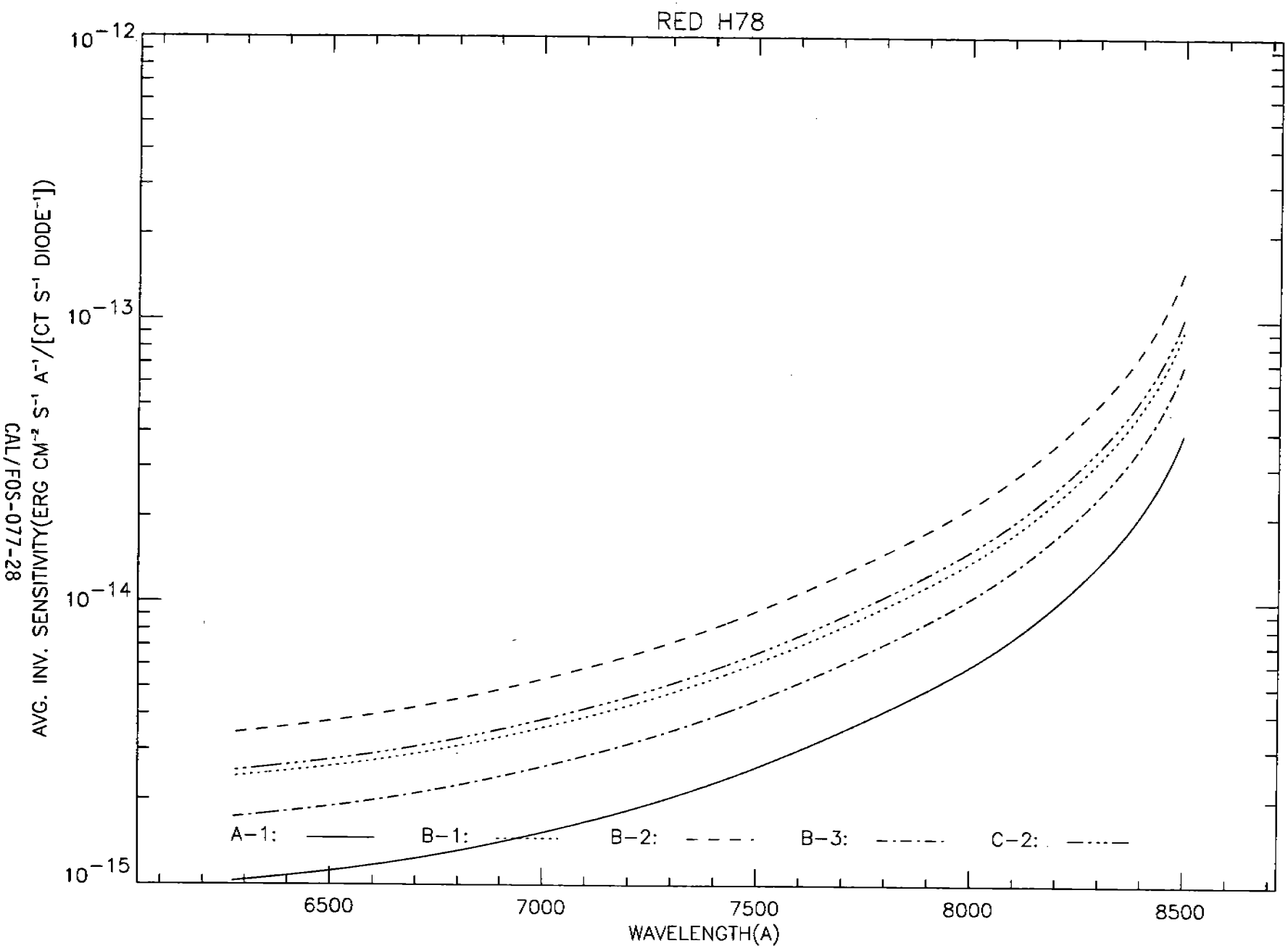
RED H78
10^{-12}
10^{-13}
10^{-14}
10^{-15}
AVG. INV. SENSITIVITY(ERG CM^{-2} S^{-1} A^{-1}/[CT S^{-1} DIODE^{-1}])
CAL/FOS-077-28
A-1:
B-1:
B-2:
B-3:
C-2:
6500
7000
7500
8000
8500
WAVELENGTH(A)

Figure 1k

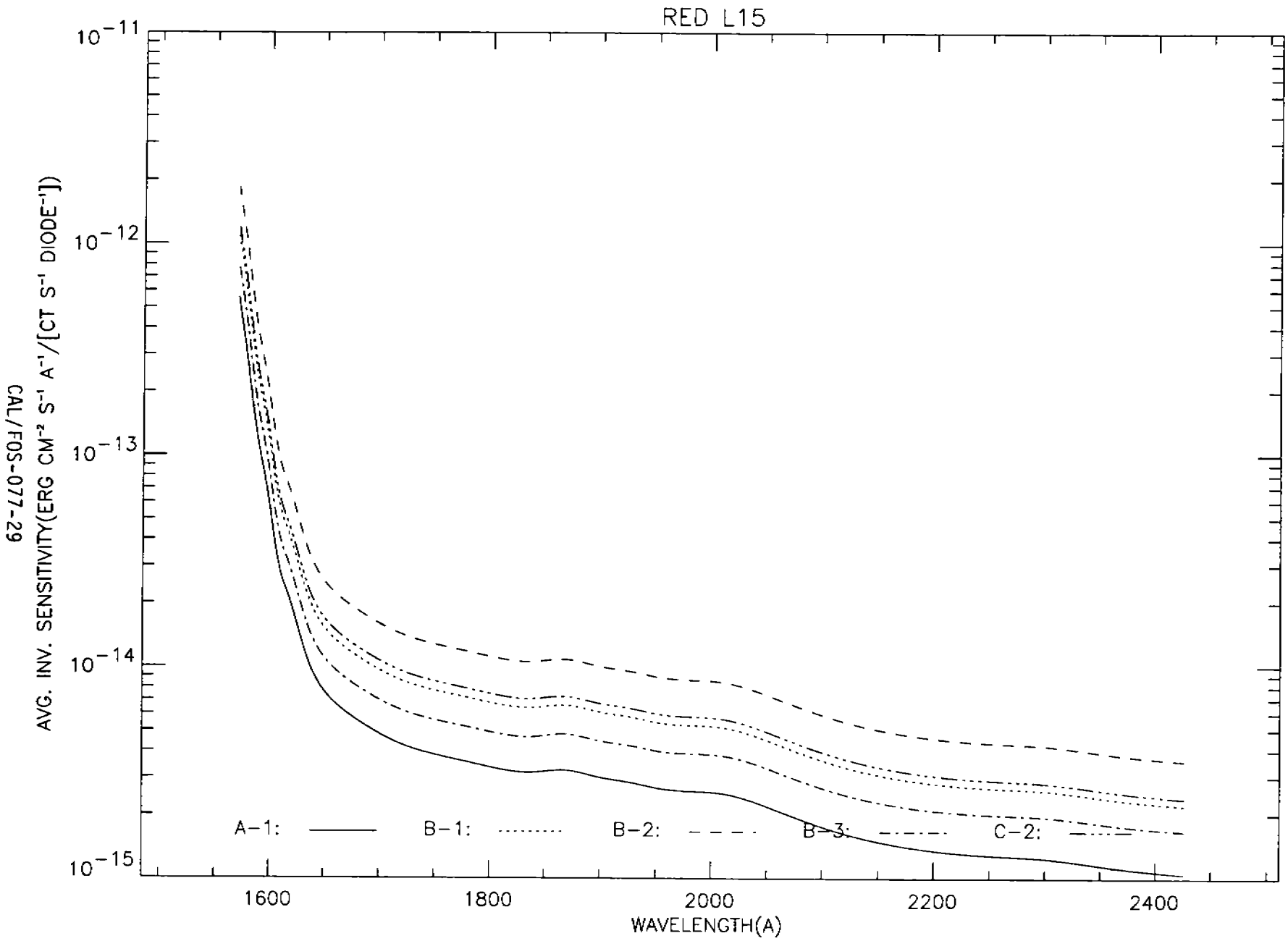
RED L15
AVG. INV. SENSITIVITY(ERG CM⁻² S⁻¹ A⁻¹/[CT S⁻¹ DIODE⁻¹])
CAL/FOS-077-29
10⁻¹¹
10⁻¹²
10⁻¹³
10⁻¹⁴
10⁻¹⁵
1600
1800
2000
2200
2400
WAVELENGTH(A)
A-1:
B-1:
B-2:
B-3:
C-2:

Figure 11

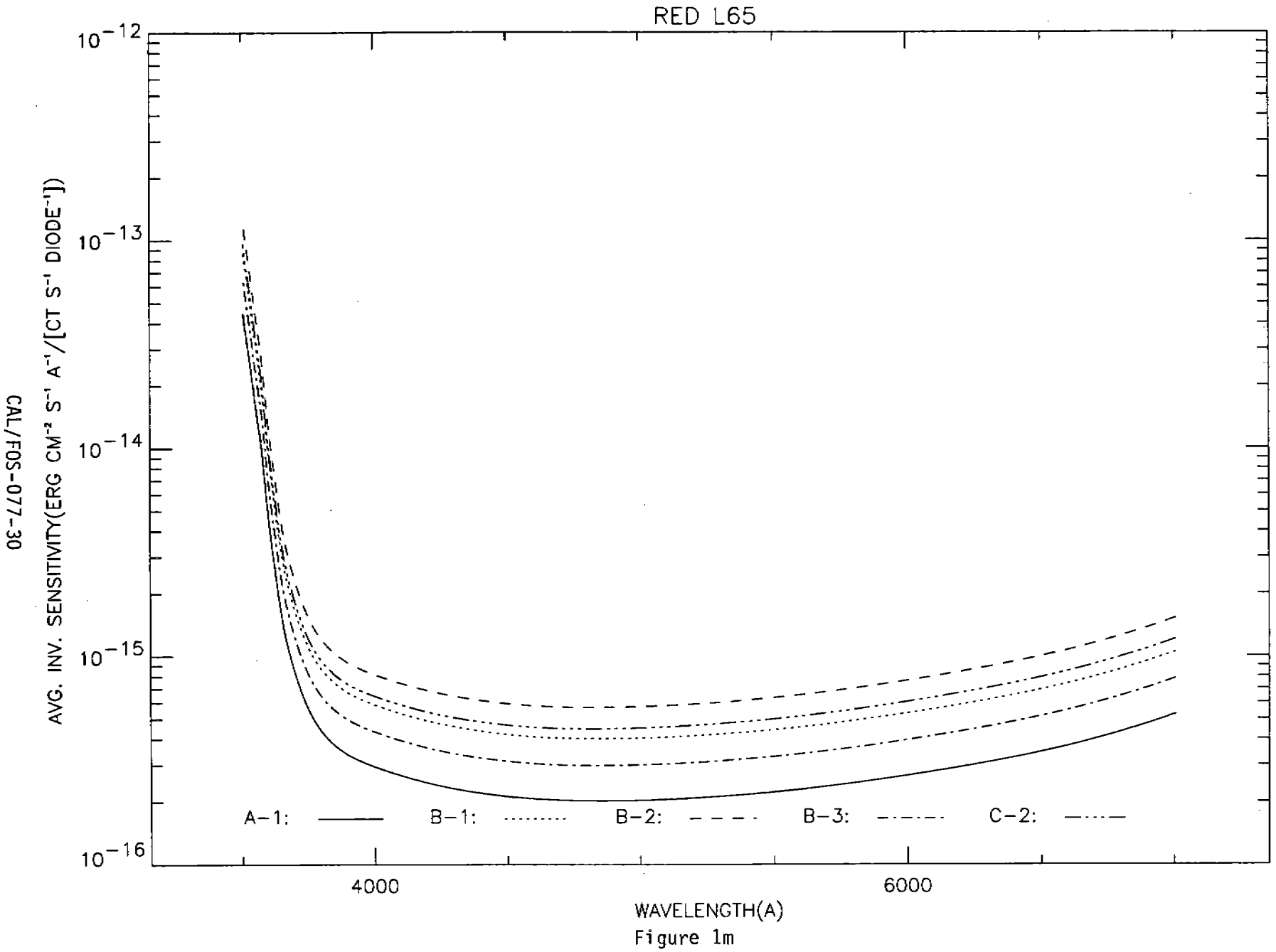
RED L65
10^{-12}
10^{-13}
10^{-14}
10^{-15}
10^{-16}
AVG. INV. SENSITIVITY(ERG CM^{-2} S^{-1} A^{-1}/[CT S^{-1} DIODE^{-1}])
CAL/FOS-077-30
A-1:
B-1:
B-2:
B-3:
C-2:
4000
6000
WAVELENGTH(A)

Figure 1m

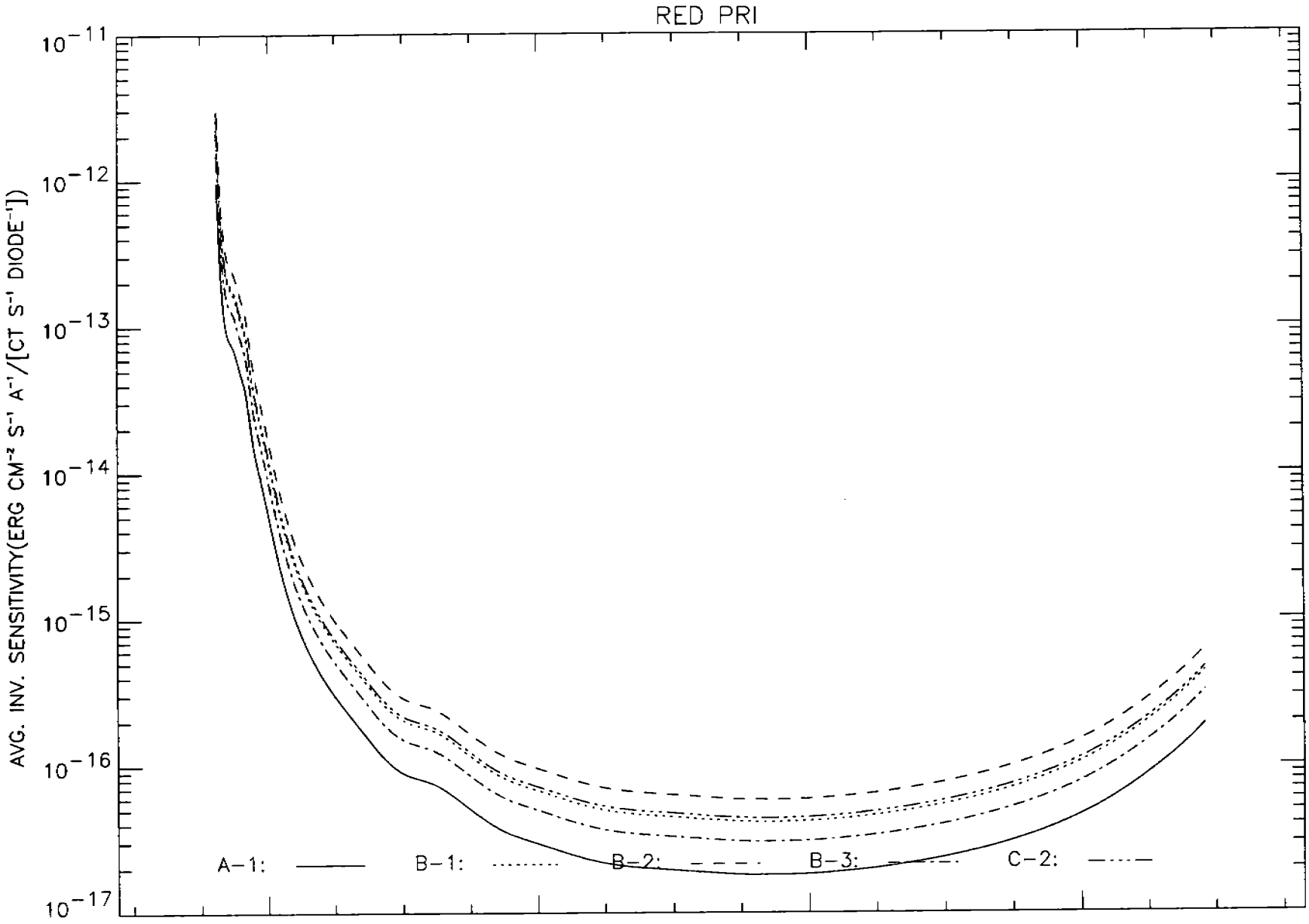

CAL/FOS-077-31

Figure 1n

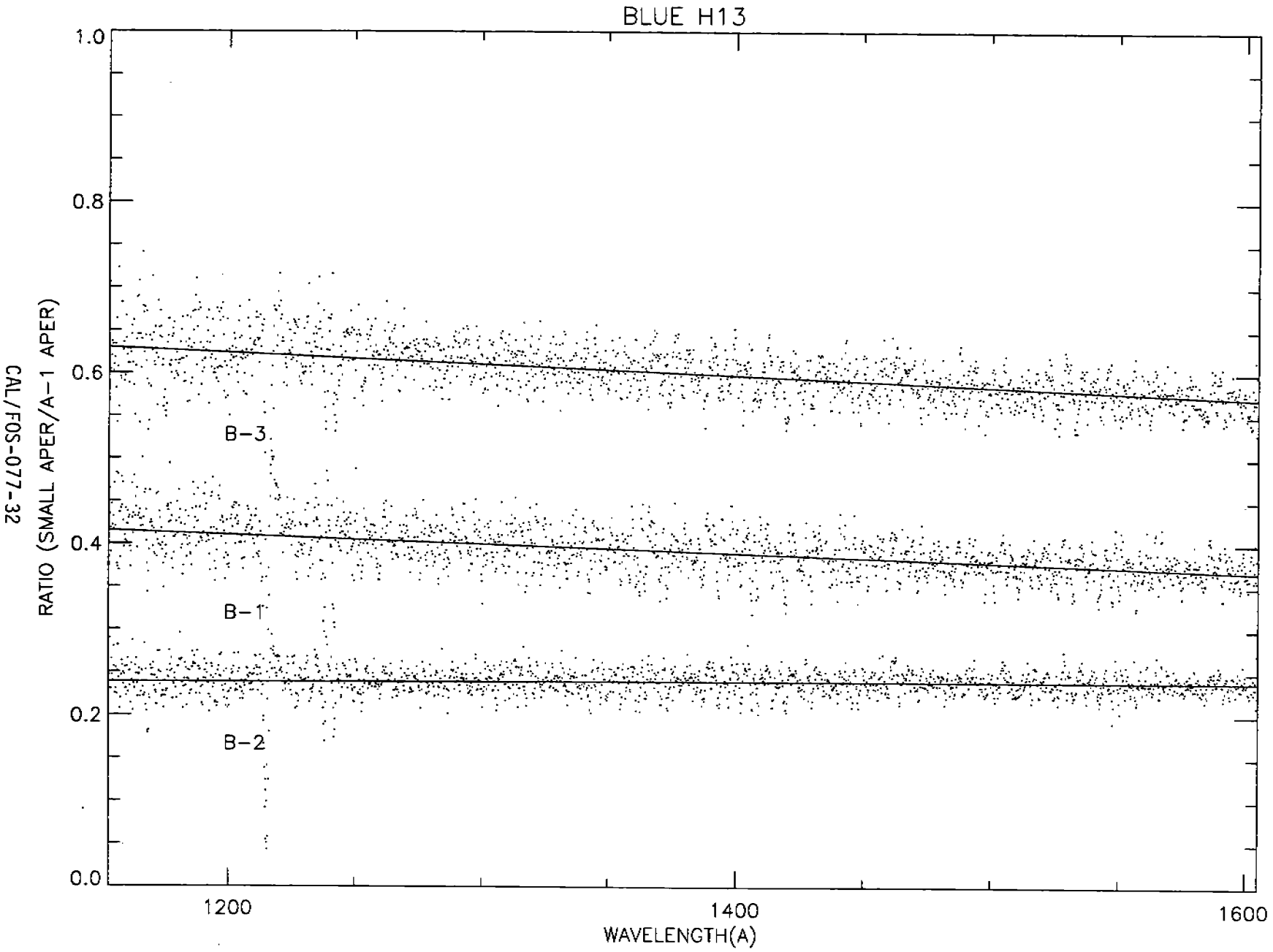
BLUE H13
1.0
0.8
0.6
0.4
0.2
0.0
RATIO (SMALL APER/A-1 APER)
CAL/FOS-077-32
B-3
B-1
B-2
1200
1400
1600
WAVELENGTH(A)

Figure 2a

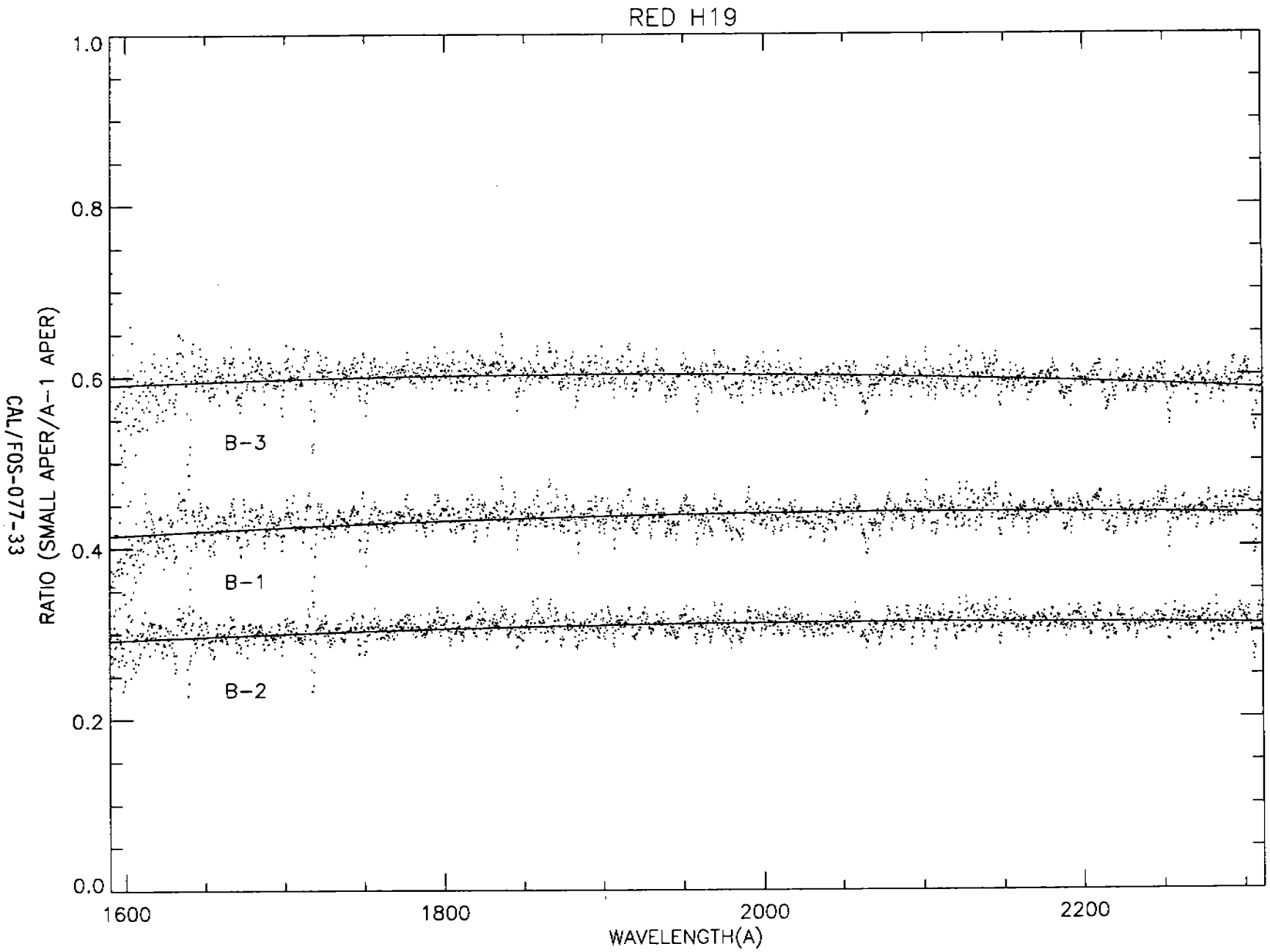
RED H19
1.0
0.8
0.6
0.4
0.2
0.0
RATIO (SMALL APER/A-1 APER)
CAL/FOS-077-33
B-3
B-1
B-2
1600
1800
2000
2200
WAVELENGTH(A)

Figure 2b

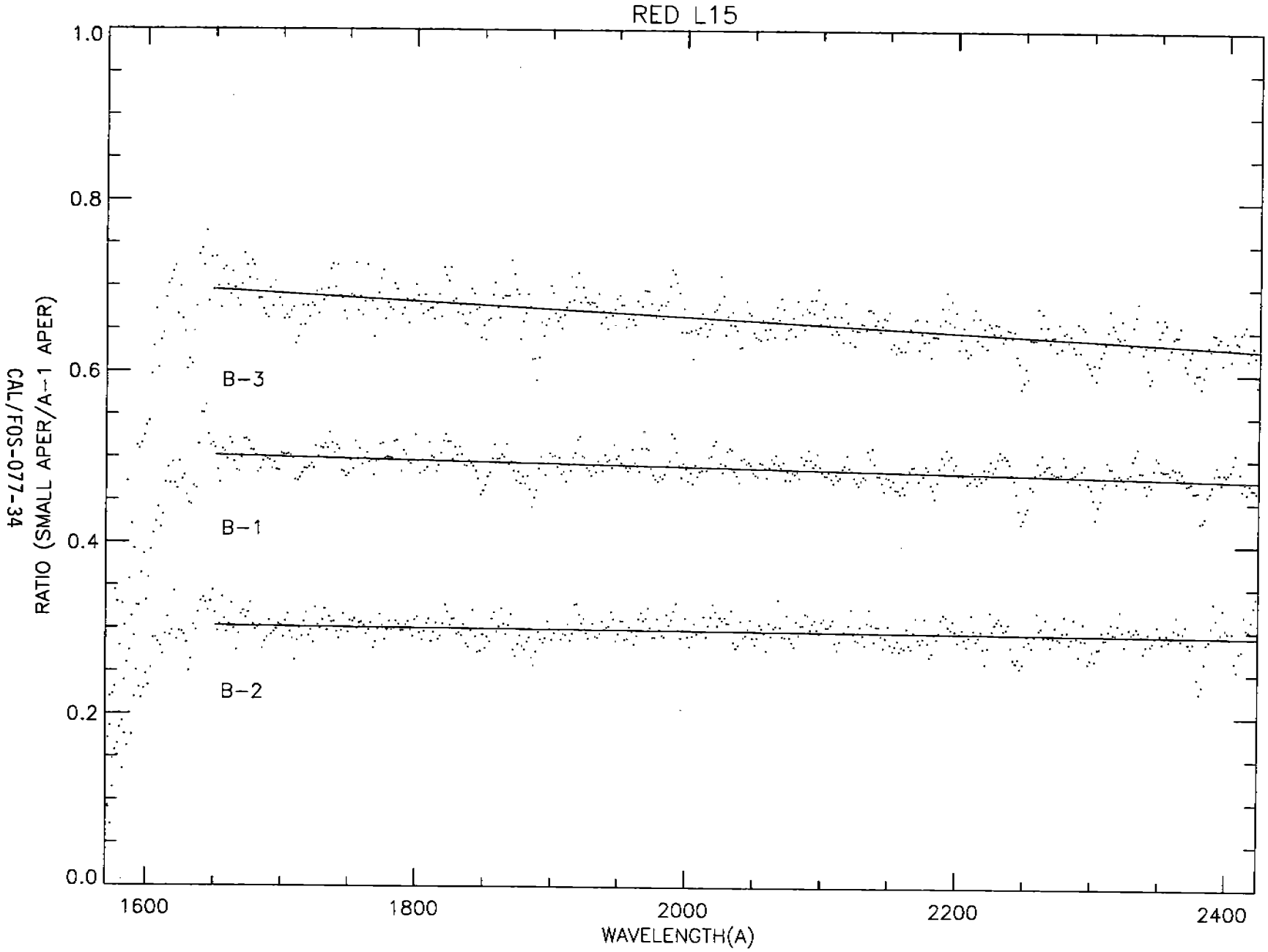
RED L15
1.0
0.8
0.6
0.4
0.2
0.0
RATIO (SMALL APER/A-1 APER)
CAL/FOS-077-34
B-3
B-1
B-2
1600
1800
2000
2200
2400
WAVELENGTH(A)

Figure 2c

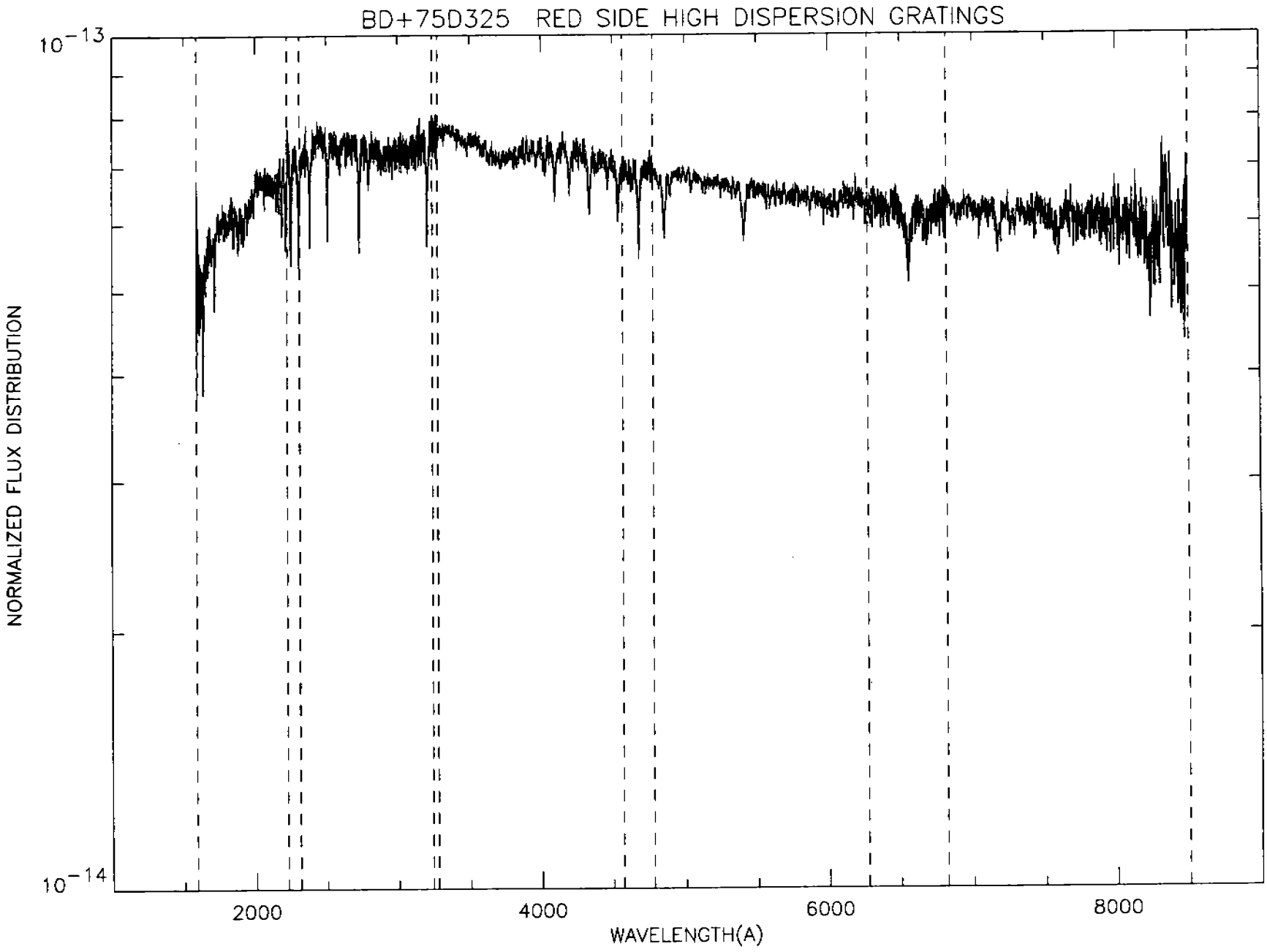
BD+75D325 RED SIDE HIGH DISPERSION GRATINGS
10^{-13}
10^{-14}
NORMALIZED FLUX DISTRIBUTION
CAL/FOS-077-35
2000
4000
6000
8000
WAVELENGTH(A)

Figure 3

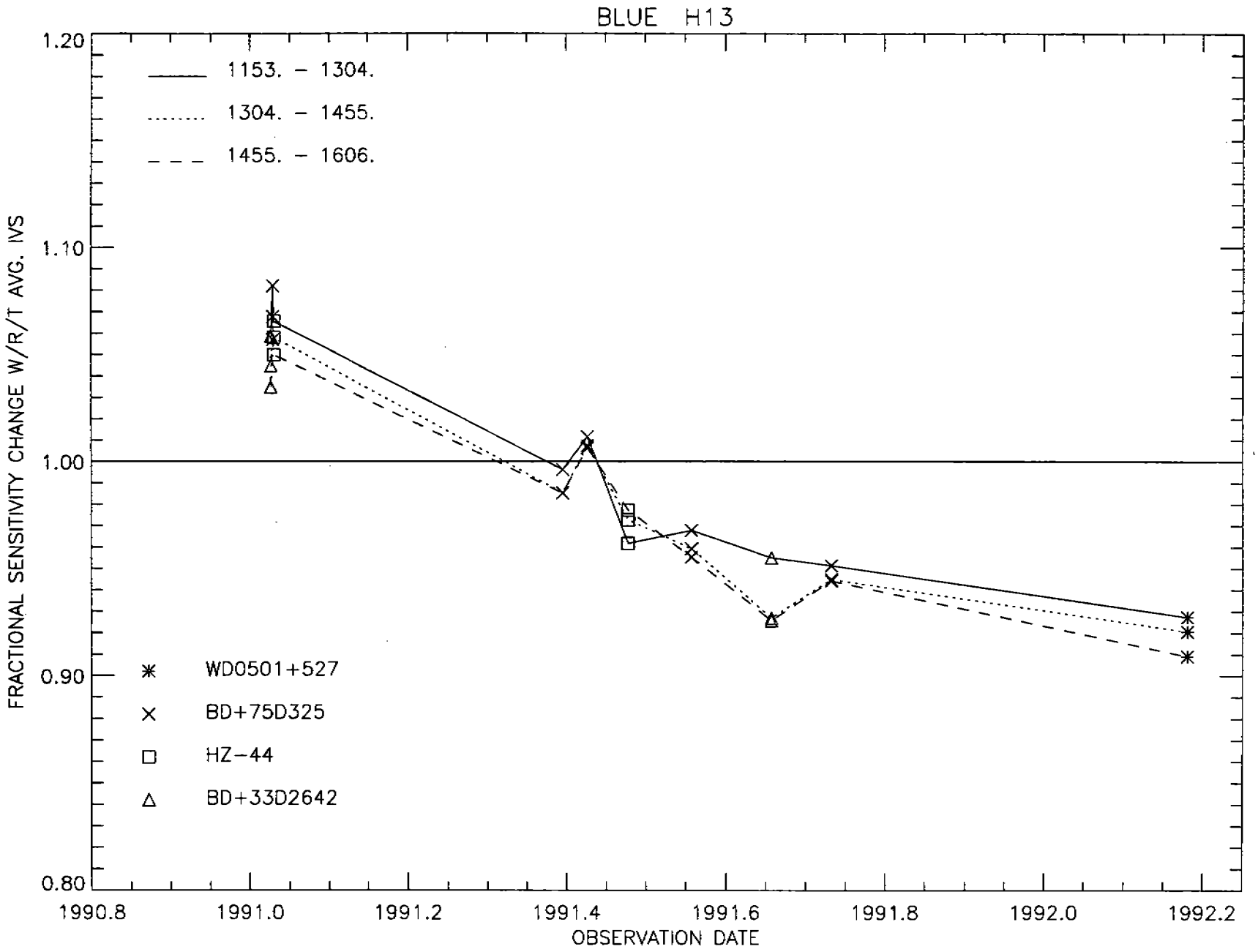
BLUE H13
1153. – 1304.
1304. – 1455.
1455. – 1606.
FRACTIONAL SENSITIVITY CHANGE W/R/T AVG. IVS
1.20
1.10
1.00
0.90
0.80
WD0501+527
BD+75D325
HZ-44
BD+33D2642
1990.8
1991.0
1991.2
1991.4
1991.6
1991.8
1992.0
1992.2
OBSERVATION DATE

Figure 4a

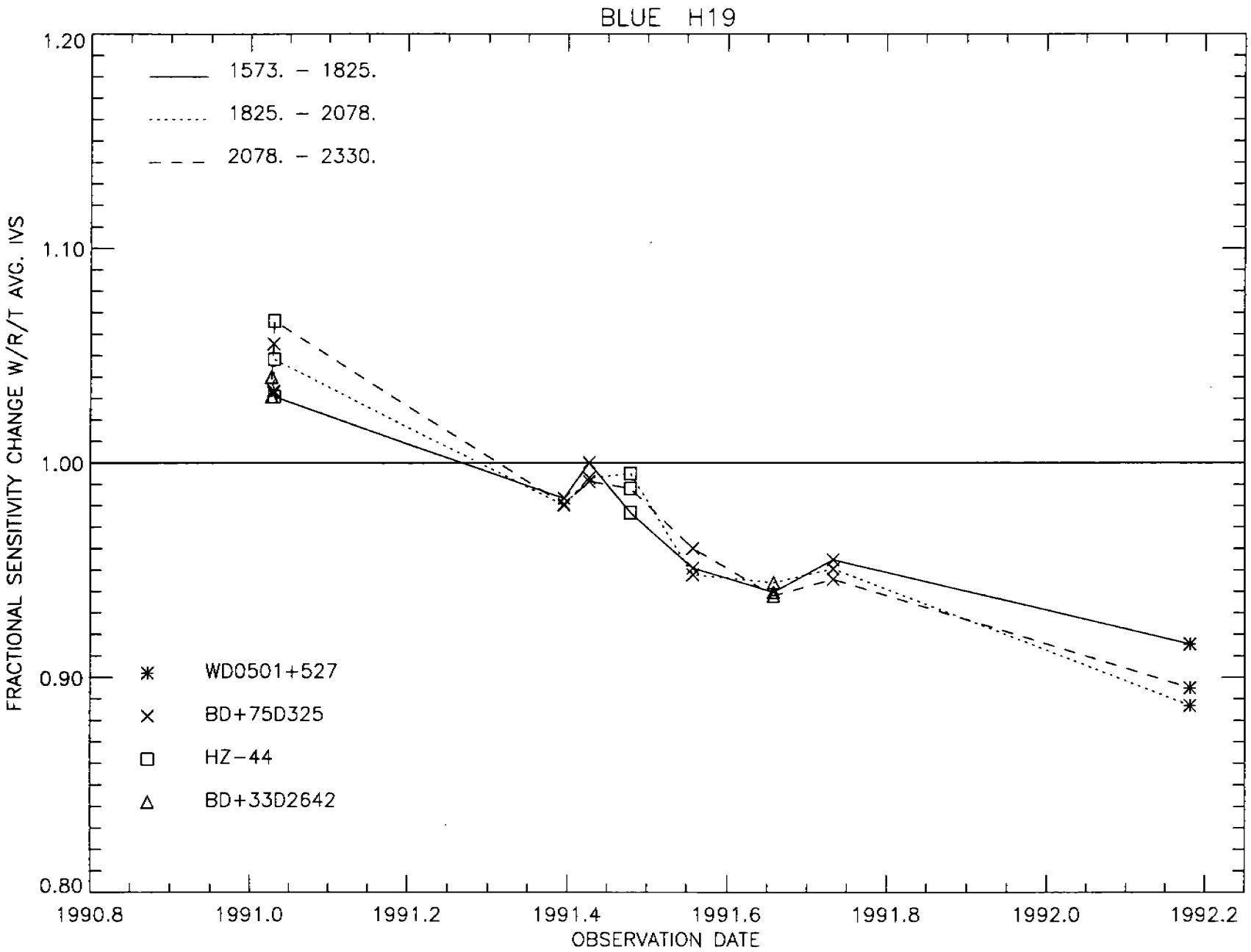
BLUE H19
1573. - 1825.
1825. - 2078.
2078. - 2330.
FRACTIONAL SENSITIVITY CHANGE W/R/T AVG. IVS
CAL/FOS-077-37
1.20
1.10
1.00
0.90
0.80
WD0501+527
BD+75D325
HZ-44
BD+33D2642
1990.8
1991.0
1991.2
1991.4
1991.6
1991.8
1992.0
1992.2
OBSERVATION DATE

Figure 4b

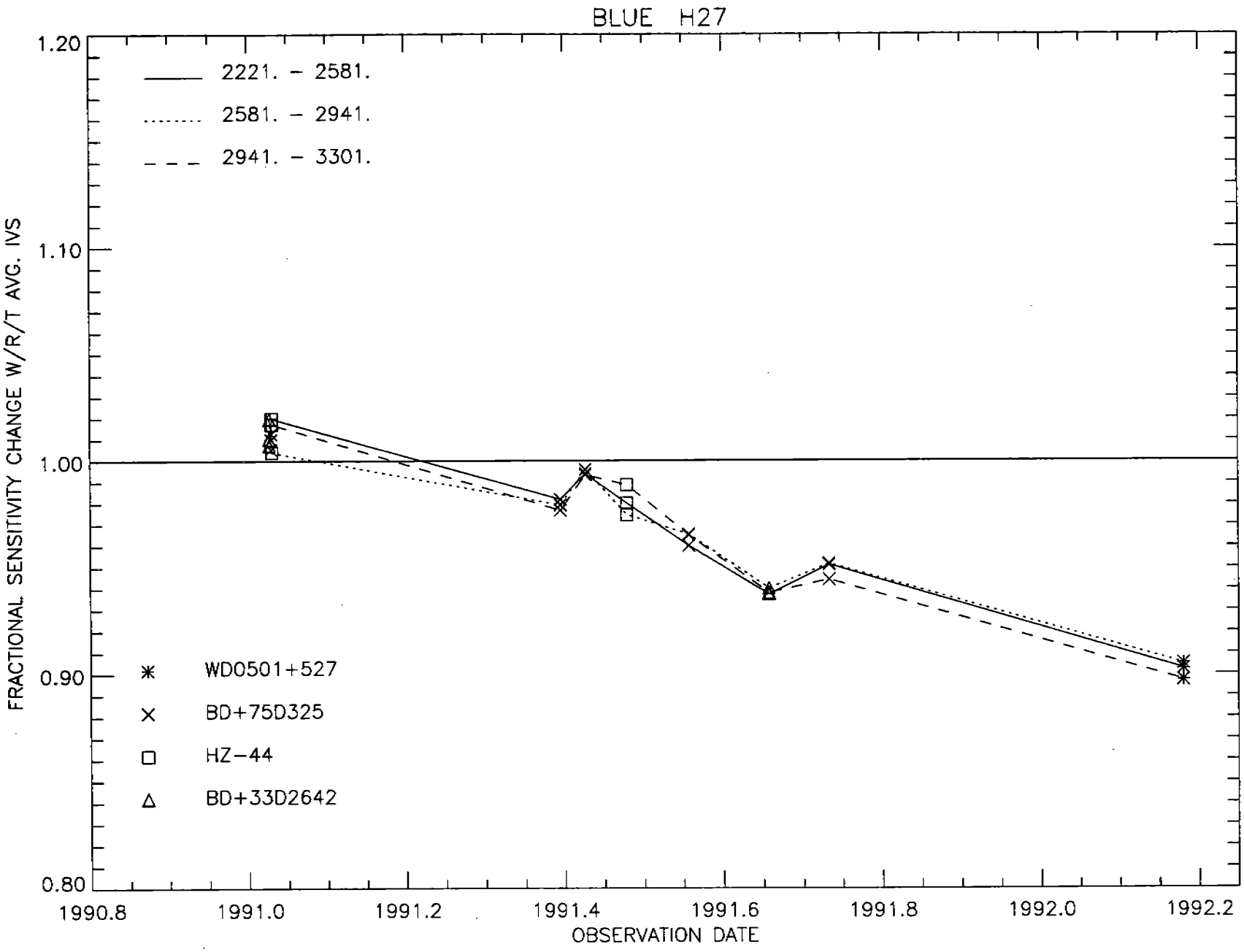
BLUE H27
2221. - 2581.
2581. - 2941.
2941. - 3301.
WD0501+527
BD+75D325
HZ-44
BD+33D2642
FRACTIONAL SENSITIVITY CHANGE W/R/T AVG. IVS
CAL/FOS-077-38
OBSERVATION DATE
1.20
1.10
1.00
0.90
0.80
1990.8
1991.0
1991.2
1991.4
1991.6
1991.8
1992.0
1992.2

Figure 4c

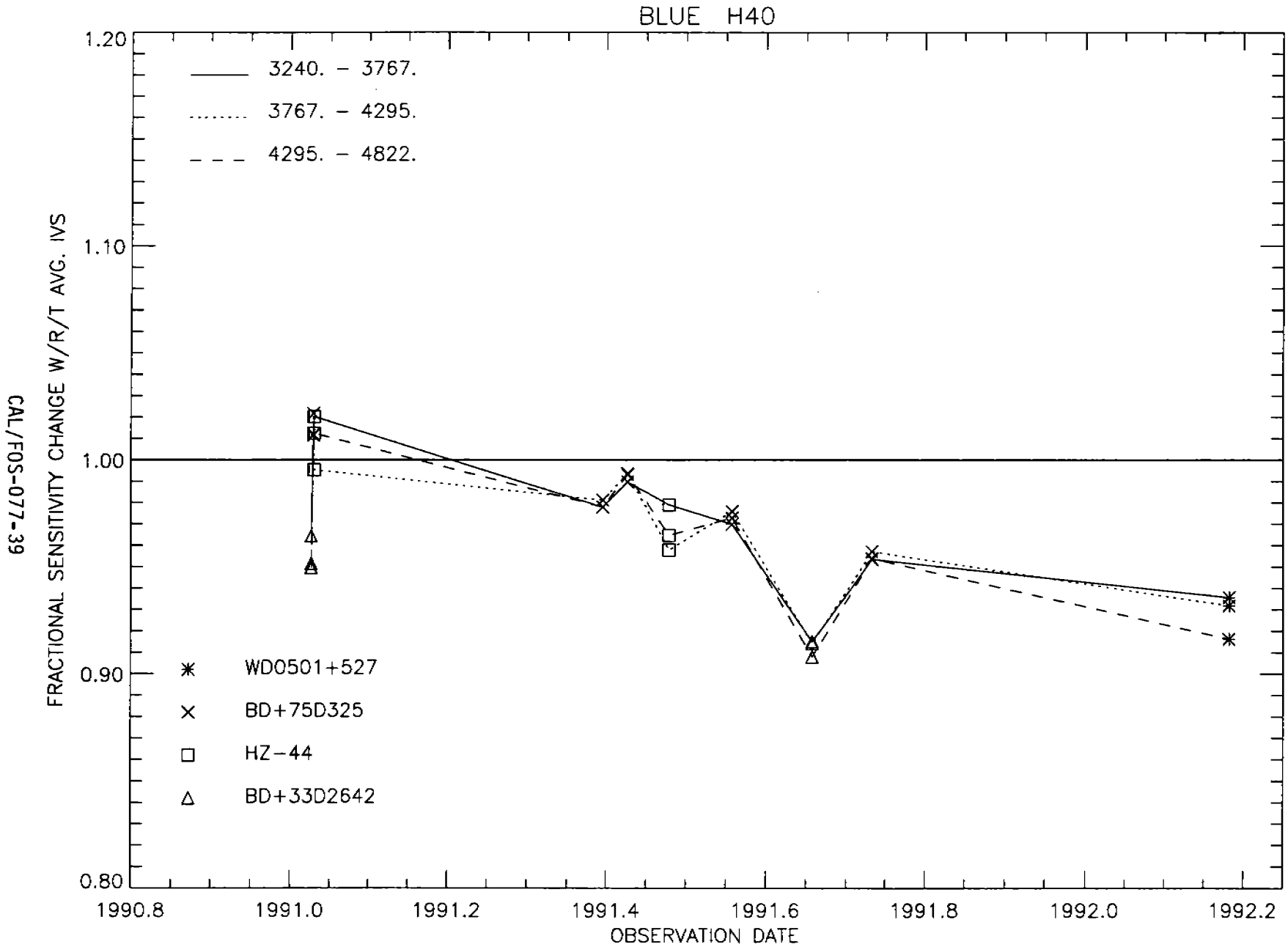
BLUE H40
3240. - 3767.
3767. - 4295.
4295. - 4822.
WD0501+527
BD+75D325
HZ-44
BD+33D2642
FRACTIONAL SENSITIVITY CHANGE W/R/T AVG. IVS
OBSERVATION DATE
1.20
1.10
1.00
0.90
0.80
1990.8
1991.0
1991.2
1991.4
1991.6
1991.8
1992.0
1992.2
CAL/FOS-077-39

Figure 4d

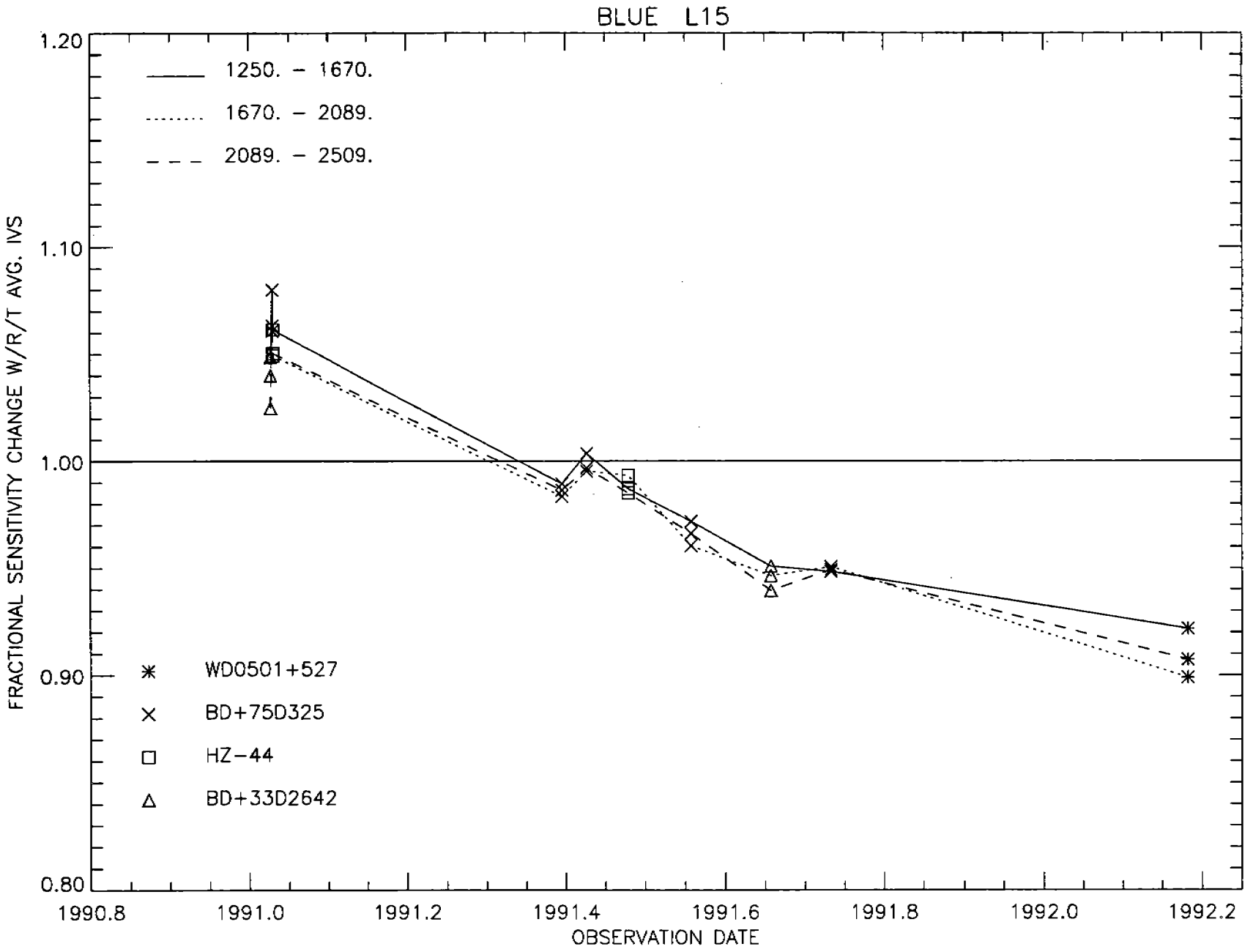
BLUE L15
1250. - 1670.
1670. - 2089.
2089. - 2509.
WD0501+527
BD+75D325
HZ-44
BD+33D2642
FRACTIONAL SENSITIVITY CHANGE W/R/T AVG. IVS
OBSERVATION DATE
1.20
1.10
1.00
0.90
0.80
1990.8
1991.0
1991.2
1991.4
1991.6
1991.8
1992.0
1992.2
CAL/FOS-077-40

Figure 4e

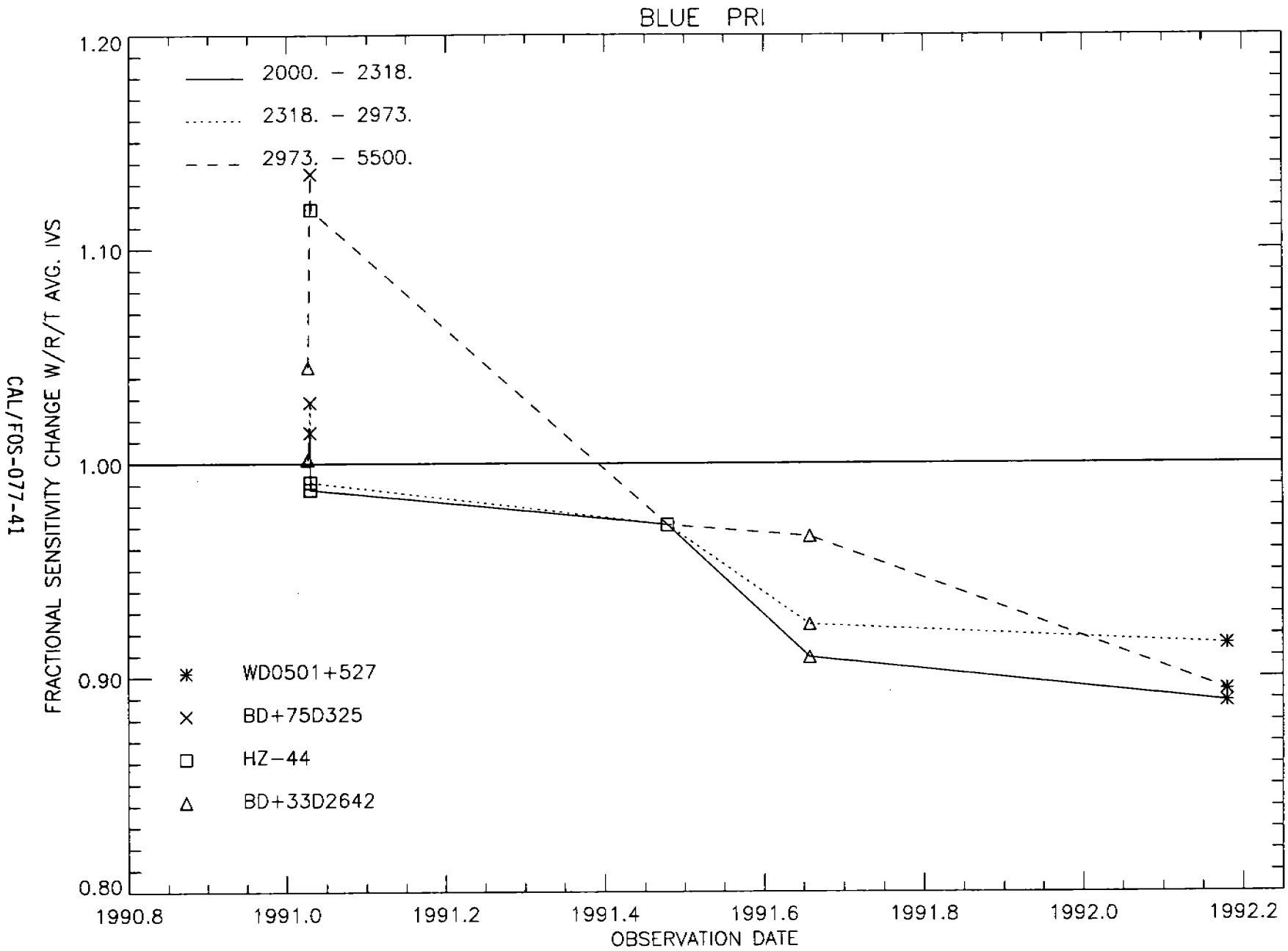
BLUE PRI
2000. – 2318.
2318. – 2973.
2973. – 5500.
WD0501+527
BD+75D325
HZ–44
BD+33D2642
FRACTIONAL SENSITIVITY CHANGE W/R/T AVG. IVS
CAL/FOS-077-41
OBSERVATION DATE
1.20
1.10
1.00
0.90
0.80
1990.8
1991.0
1991.2
1991.4
1991.6
1991.8
1992.0
1992.2

Figure 4f

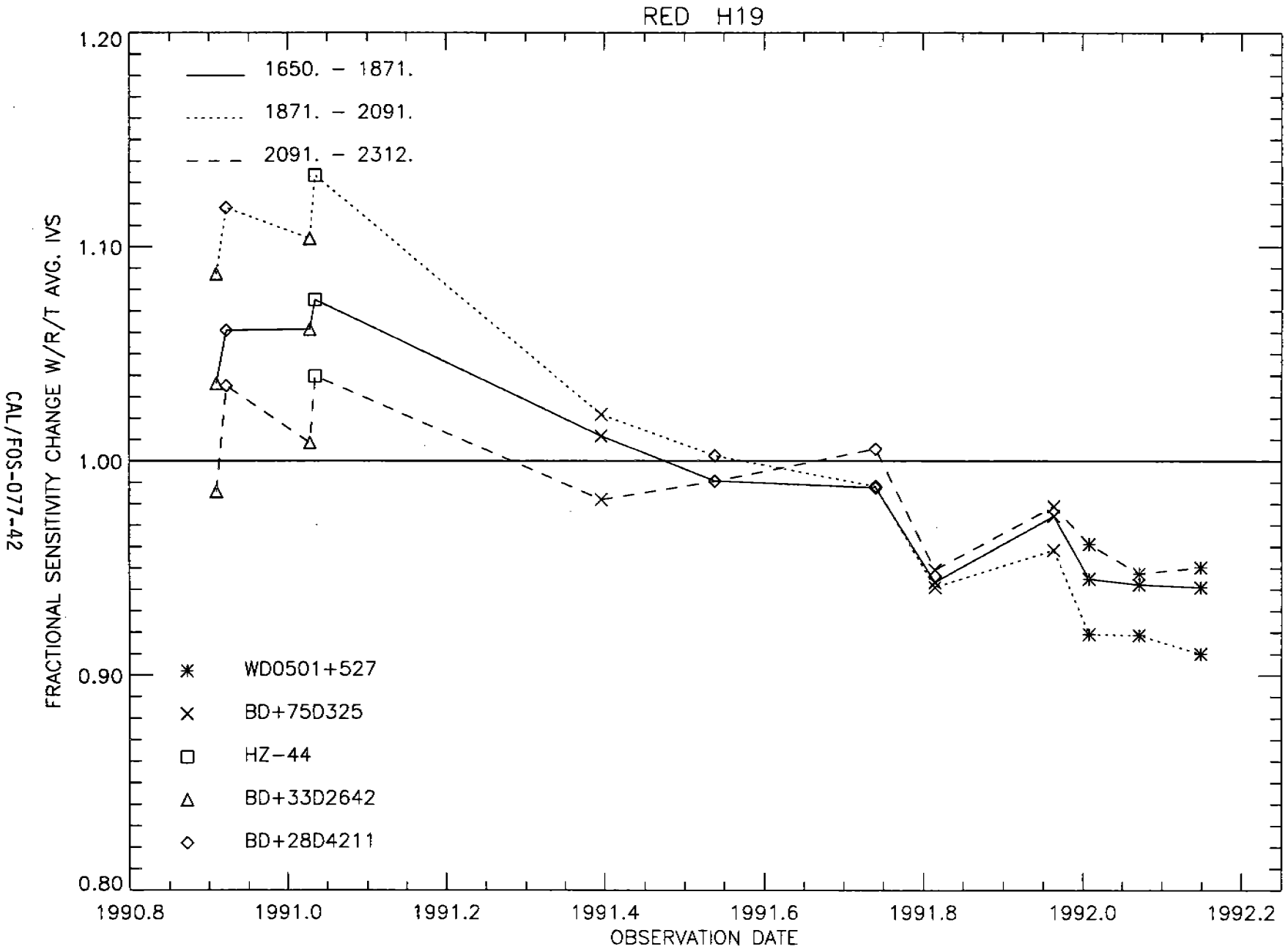

CAL/FOS-077-42

Figure 4g

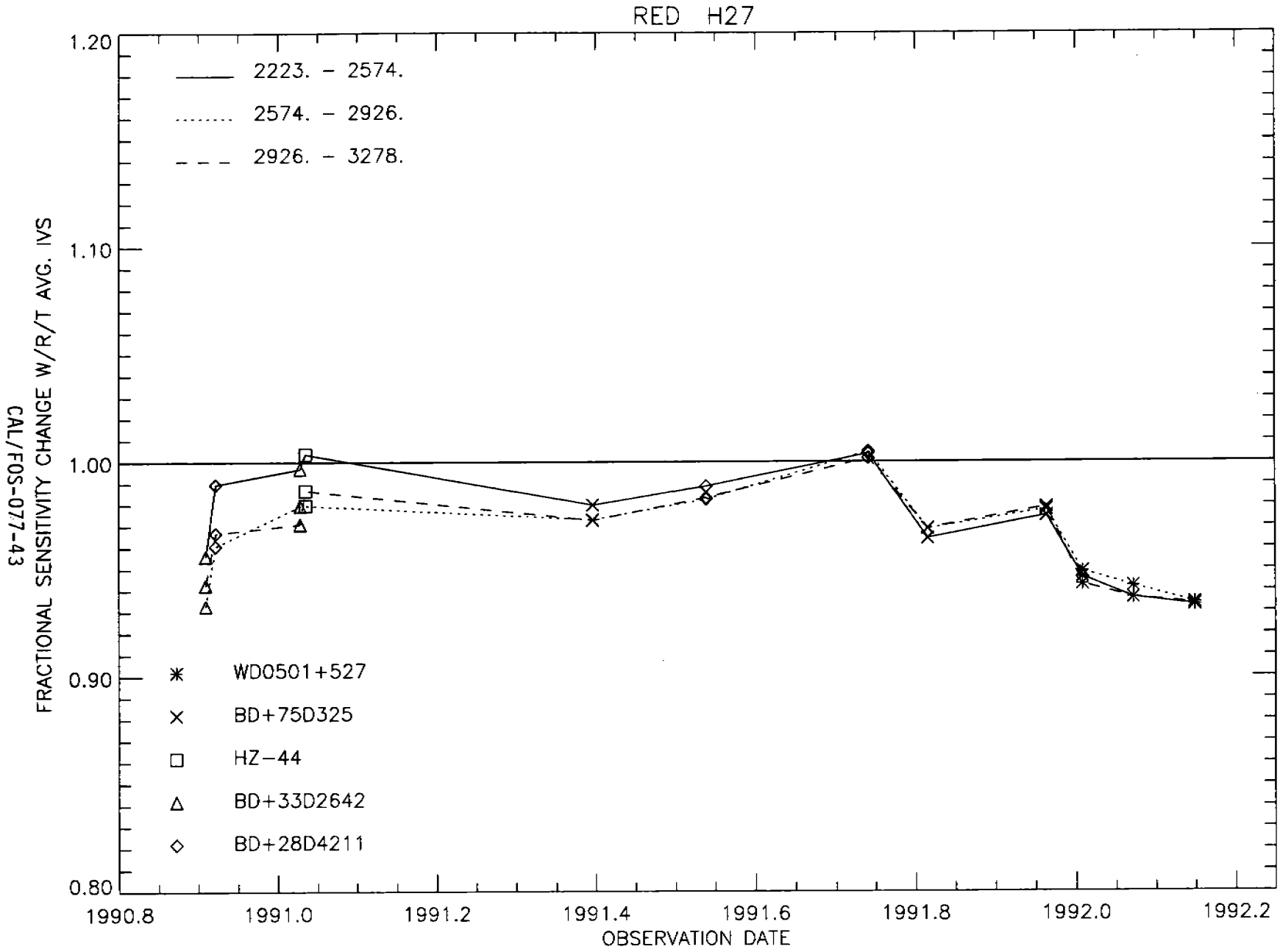
RED H27
2223. - 2574.
2574. - 2926.
2926. - 3278.
WD0501+527
BD+75D325
HZ-44
BD+33D2642
BD+28D4211
FRACTIONAL SENSITIVITY CHANGE W/R/T AVG. IVS
CAL/FOS-077-43
OBSERVATION DATE
1.20
1.10
1.00
0.90
0.80
1990.8
1991.0
1991.2
1991.4
1991.6
1991.8
1992.0
1992.2

Figure 4h

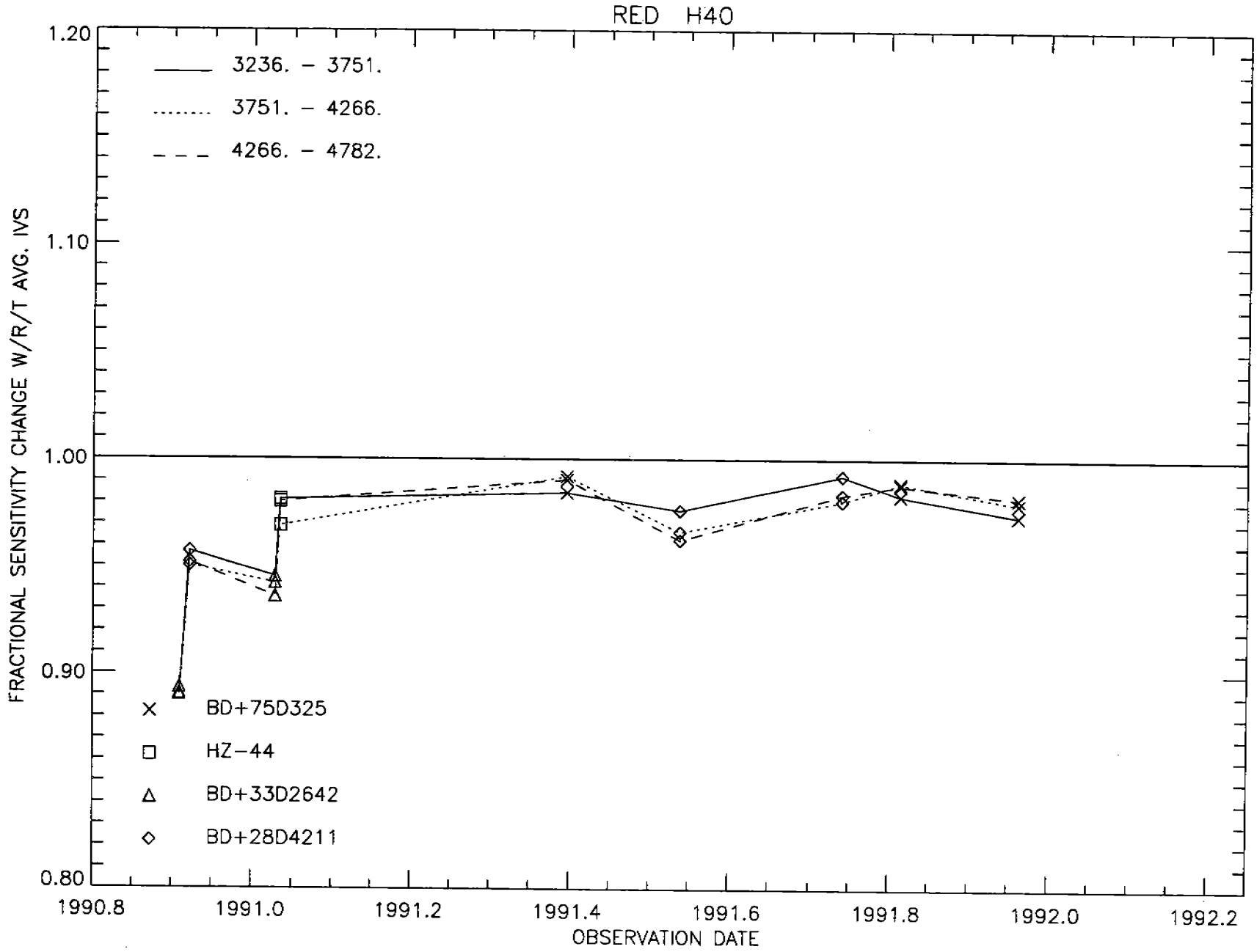
RED H40
3236. - 3751.
3751. - 4266.
4266. - 4782.
FRACTIONAL SENSITIVITY CHANGE W/R/T AVG. IVS
CAL/FOS-077-44
1.20
1.10
1.00
0.90
0.80
BD+75D325
HZ-44
BD+33D2642
BD+28D4211
1990.8
1991.0
1991.2
1991.4
1991.6
1991.8
1992.0
1992.2
OBSERVATION DATE

Figure 4i

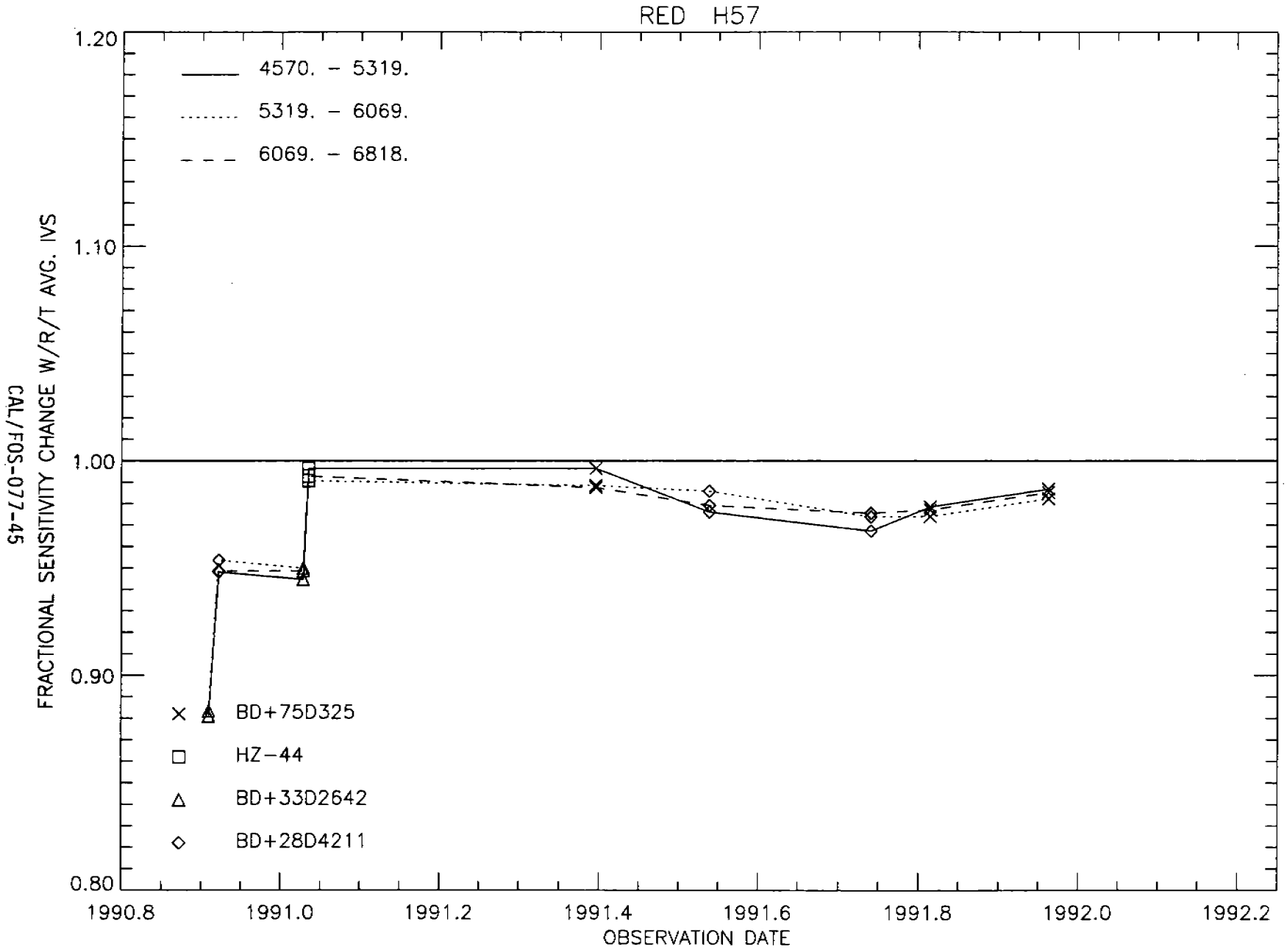
RED H57
4570. - 5319.
5319. - 6069.
6069. - 6818.
1.20
1.10
1.00
0.90
0.80
FRACTIONAL SENSITIVITY CHANGE W/R/T AVG. IVS
CAL/FOS-077-45
BD+75D325
HZ-44
BD+33D2642
BD+28D4211
1990.8
1991.0
1991.2
1991.4
1991.6
1991.8
1992.0
1992.2
OBSERVATION DATE

Figure 4j

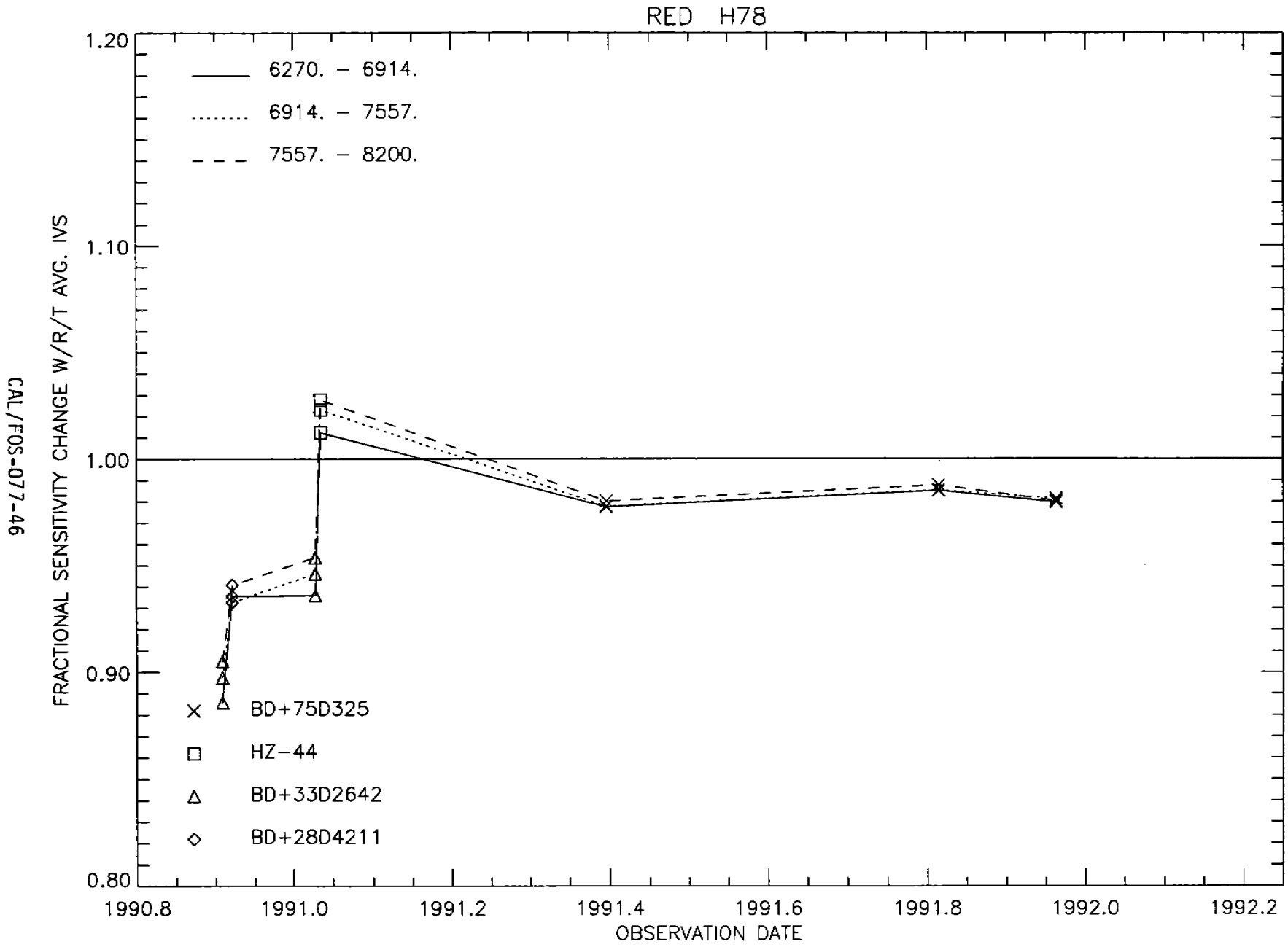
RED H78
6270. – 6914.
6914. – 7557.
7557. – 8200.
FRACTIONAL SENSITIVITY CHANGE W/R/T AVG. IVS
CAL/FOS-077-46
1.20
1.10
1.00
0.90
0.80
BD+75D325
HZ–44
BD+33D2642
BD+28D4211
1990.8
1991.0
1991.2
1991.4
1991.6
1991.8
1992.0
1992.2
OBSERVATION DATE

Figure 4k

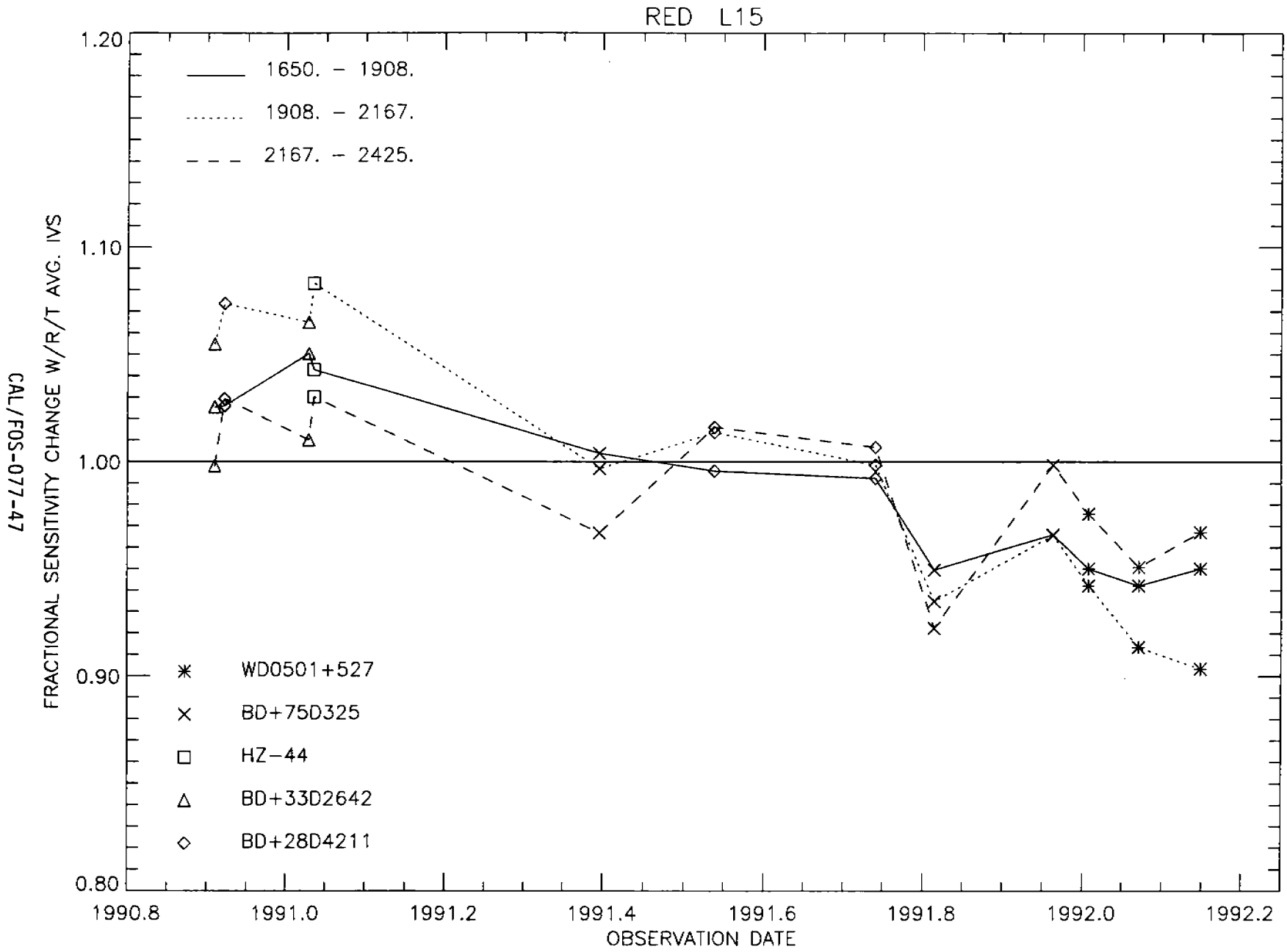
RED L15
1650. - 1908.
1908. - 2167.
2167. - 2425.
WD0501+527
BD+75D325
HZ-44
BD+33D2642
BD+28D4211
FRACTIONAL SENSITIVITY CHANGE W/R/T AVG. IVS
CAL/FOS-077-47
OBSERVATION DATE
1.20
1.10
1.00
0.90
0.80
1990.8
1991.0
1991.2
1991.4
1991.6
1991.8
1992.0
1992.2

Figure 41

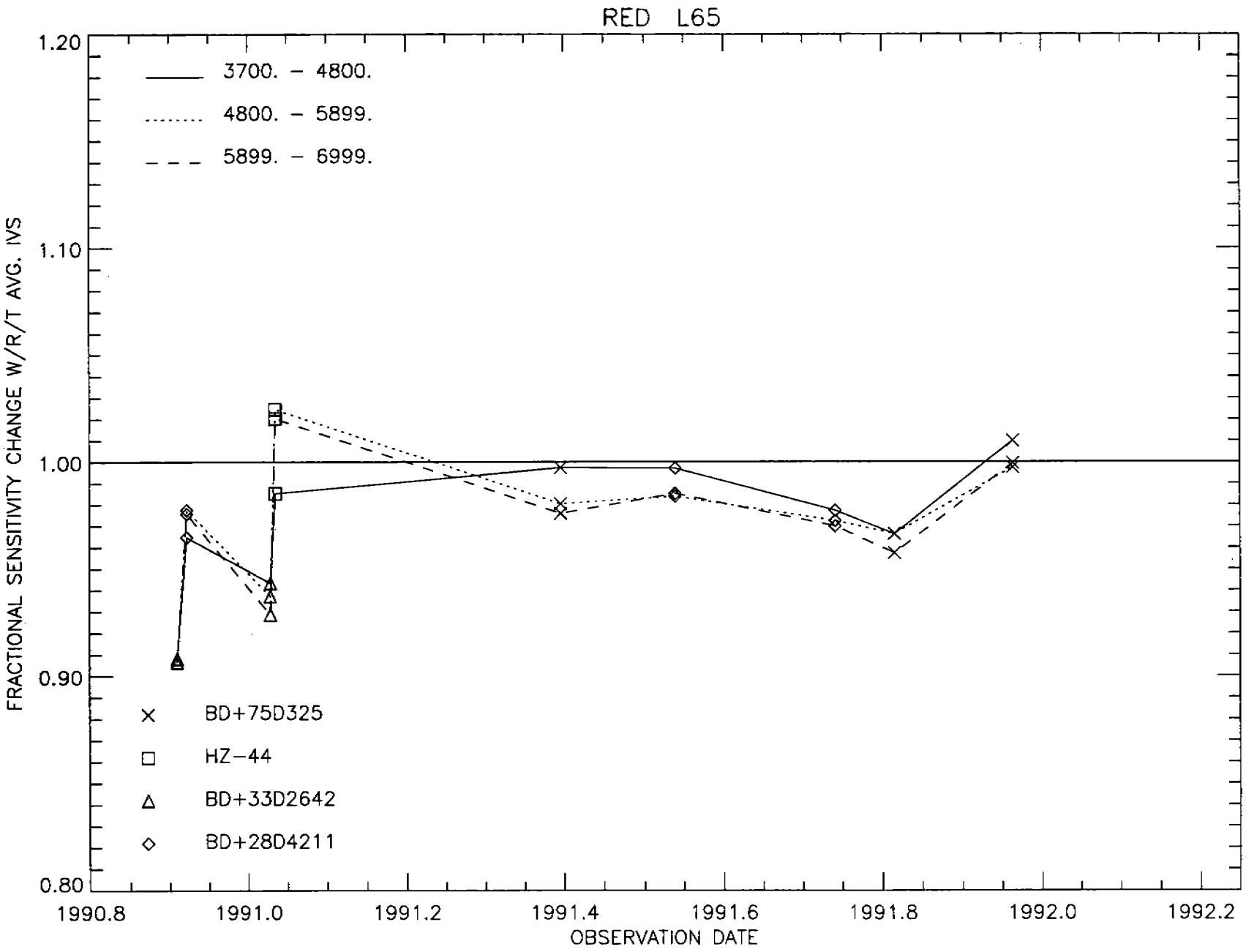

CAL/FOS-077-48

Figure 4m

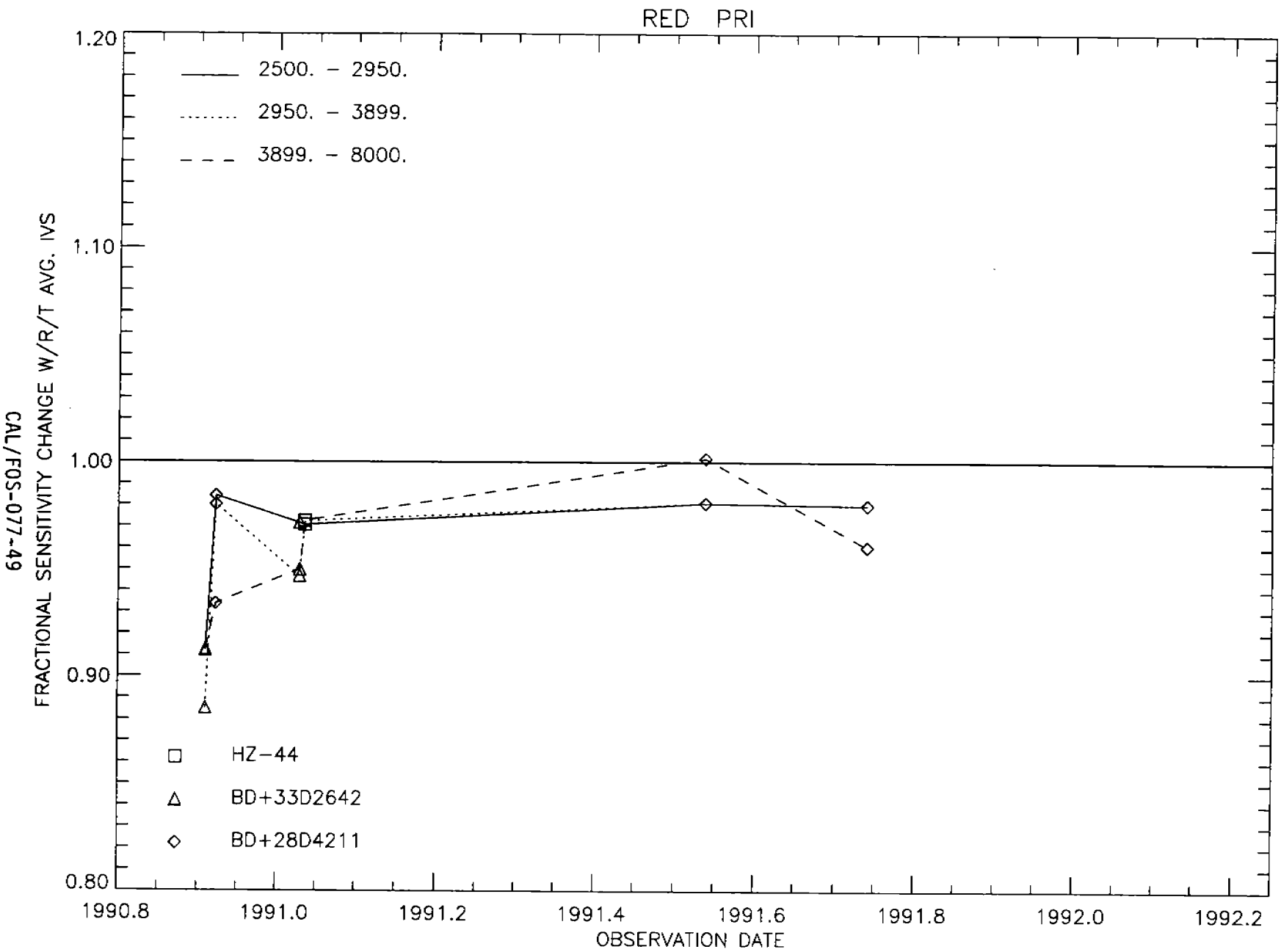
RED PRI
2500. - 2950.
2950. - 3899.
3899. - 8000.
FRACTIONAL SENSITIVITY CHANGE W/R/T AVG. IVS
CAL/FOS-077-49
1.20
1.10
1.00
0.90
0.80
1990.8
1991.0
1991.2
1991.4
1991.6
1991.8
1992.0
1992.2
OBSERVATION DATE
HZ-44
BD+33D2642
BD+28D4211

Figure 4n